Electrochemical Co-Production of Hydrogen, Base and Acid from Low-value Brines via Direct Electrosynthesis

A Thesis

Presented to the Faculty of the Graduate School

of Cornell University

In Partial Fulfillment of the Requirements for the Degree of

Master of Science

by

Minkyeong Kim

August 2023

ABSTRACT

Hydrogen production is of growing interest as a low-carbon alternative fuel. However, most of the hydrogen is still produced from fossil fuels. In contrast, brine electrolysis offers a promising route to produce hydrogen and other valuable byproducts. However, the conventional method for producing acid and base simultaneously using bipolar-membrane electrodialysis (BMED), consumes significant energy and has a complexed configuration. Additionally, it is important to suppress chlorine evolution and produce HCl instead in brine electrolysis. This study investigates the performance and economic viability of three different brine electrolysis systems: direct electrosynthesis (DE) without a bipolar-membrane, anion exchange membrane (AEM), and cation exchange membrane (CEM) systems, using a new Manganese-Molybdenum coated titanium electrode that suppresses Cl_2. Results show that the DE-MnMo/Ti electrode system produced 0.005 mol of H_2, 0.0041 mol of O_2, 0.37 M NaOH, and 0.2 M HCl. Compared to pure water electrolysis, brine electrolysis offers higher economic potential due to the production of value-added products such as O_2, NaOH and HCl. Using the DE-MnMo/Ti electrode system and brine, the revenue generated per year is 4 times higher than that of alkaline electrolysis using pure water. Additionally, a life cycle assessment (LCA) is conducted to evaluate the environmental impacts of the DE-MnMo/Ti system. The LCA analysis showed that the DE-MnMo/Ti system can reduce greenhouse gas emissions, energy use, and water usage. Therefore, this study highlights the potential for brine electrolysis with the DE-MnMo/Ti electrode system as an economically viable and environmentally sustainable route for producing hydrogen and high value co-products such as NaOH, HCl, and O_2.

BIOGRAPHICAL SKETCH

Minkyeong Kim holds a bachelor's degree in resource and environmental Engineering from Hanyang University in Korea. During her undergraduate studies, she gained a strong foundation in Resource and Environmental Engineering. This background gave her the opportunity to advance energy production technologies in her first job at Korea Gas Corporation (KOGAS).

As a member of the LNG development team at KOGAS, she played an integral role in managing and developing the company's LNG business. Her responsibilities included overseeing the development of new LNG projects, managing the financial aspects of the business, and ensuring the smooth operation of existing projects. Minkyeong's time at KOGAS allowed her to hone her business and management skills, which she would later leverage in her academic pursuits. Her passion for advancing sustainable energy conversion solutions motivated her to pursue a master's degree in civil and environmental engineering at Cornell University.

During her time at Cornell University, Minkyeong focused on advancing sustainable pathways to produce low carbon energy carriers such as H_2 from low value resources. These pathways will play a key role in the transition to a clean energy future. Minkyeong's research has also given her a deep understanding of the energy industry and the challenges that lie ahead.

As she approaches graduation, she is excited to take the knowledge and experience gained at Cornell University and apply it to her work at KOGAS. Her goal is to plan and execute a real hydrogen project that can contribute to the development of a more sustainable energy industry. She knows that the journey ahead will be challenging, but she is confident that her education and experience have prepared her well for the task.

ACKNOWLEDGMENTS

During my two years of master's degree at Cornell University, I came to realize that no great achievements are accomplished alone, but rather they are the culmination of the help and support provided by numerous people. I am grateful to have had the opportunity to be surrounded by so many wonderful individuals who have contributed to my growth.

First and foremost, I would like to express my heartfelt gratitude to my advisor, Professor Greeshma Gadikota, for her unwavering support and guidance throughout my research journey. From the moment I arrived in Ithaca, she has been a source of inspiration and motivation for me. Her profound knowledge, insightful feedback, and constructive criticism have helped me to stay focused and make progress even when faced with difficult challenges. Without her direction and guidance, I would not have been able to complete my research project.

I would also like to extend my sincere appreciation to Special Committee member Professor Jacob Paul Mays for his valuable contribution to my education. Through his course, I gained a deeper understanding of the energy power market and the concept of economic feasibility, which was highly relevant to my research on evaluating the economics of hydrogen production. His wisdom and expertise have been instrumental in shaping my academic and professional career.

I would also like to express my gratitude to Professor Tobias Hanrath for serving as a committee member. His course on energy storage pathways provided me with a deep understanding of the advantages and opportunities in using hydrogen as an energy storage medium and the approaches in which H_2 can be used in fuel cells that utilize it for energy generation. His knowledge and experience in fuel cells greatly assisted me in my research, and I am truly grateful for his guidance and support.

I am also grateful to all the members of the research group who have played a significant role in my growth and development. I am deeply indebted to my friend Peilong Lu, who generously shared his electrochemical expertise and provided valuable advice whenever I encountered difficulties in my research. I also deeply grateful to Demola Ogunnaike for conducting the LCA analysis of the H_2 conversion pathways that I developed and improving the quality of thesis by analyzing the environmental aspects of my research. Additionally, I am grateful for the fellowship and support provided by my classmates and colleagues in the lab, who have made my time at Cornell truly unforgettable. I would like to express my gratitude to Prince Ochonma for proofreading the manuscript of this thesis. I am especially thankful for his insightful questions regarding fundamental principles, as they have greatly contributed to improving the clarity of this thesis.

Furthermore, I would like to express my gratitude to Korea Gas Corporation (KOGAS) for their generous support in providing me with Master Sponsorship. Without their sponsorship, I would not have been able to take advantage of the valuable

opportunities and experiences that Cornell University has to offer. I am truly grateful for their support and trust in my abilities.

Finally, I would like to thank my family, mother, Dongmin Kim, and father, Dongkwon Choi, for their unconditional love, encouragement, and support throughout my journey. Their constant spiritual and emotional support has been a tremendous source of inspiration for me, and without their care and understanding, my progress and achievements would not have been possible. In conclusion, I am extremely grateful to all the people who have contributed to my success and growth during my master's degree at Cornell University. Their support, guidance, and encouragement have been instrumental in shaping my academic and professional journey, and I will always be indebted to them.

TABLE OF CONTENTS

LIST OF FIGURES

Figure 12. Comparison of HCl concentration at Pt and MnMo/Ti anodes in different electrolysis systems (a) Concentration of HCl produced at the Pt and MnMo/Ti anodes in Direct Electrolysis (DE), Anion Exchange Membrane Electrolysis (AEM) and Cation Exchange Membrane Electrolysis (CEM) systems (b) Normalized concentration of HCl produced at the Pt and MnMo/Ti anodes in Direct Electrolysis (DE), Anion Exchange Membrane Electrolysis (AEM) and Cation Exchange Membrane Electrolysis (CEM) systems.

Figure 13. Comparison of hydrogen volume at Pt and MnMo/Ti anodes in different electrolysis systems (a) Hydrogen volume produced at the Pt and MnMo/Ti anodes for Direct Electrolysis (DE), Anion Exchange Membrane Electrolysis (AEM) and Cation Exchange Membrane Electrolysis (CEM) system (b) Normalized hydrogen volume produced at the Pt and MnMo/Ti anodes for Direct Electrolysis (DE), Anion Exchange Membrane Electrolysis (AEM) and Cation Exchange Membrane Electrolysis (CEM) systems.

Figure 14. Efficiencies of oxygen evolution at the Pt and MnMo/Ti anodes for Direct Electrolysis (DE), Anion Exchange Membrane Electrolysis (AEM) and Cation Exchange Membrane Electrolysis (CEM) systems.

Figure 15. Comparison of theoretical and experimental energy consumption for NaOH production using Bipolar-Membrane Electrodialysis (BMED), Direct Electrolysis (DE), Anion Exchange Membrane Electrolysis (AEM) and Cation Exchange Membrane Electrolysis (CEM) systems. Experimental energy consumption for BMED was determined by Reig et al[20]. Theoretical estimates for DE, AEM and CEM are based on voltages, and they are reported by Kumar et al[24].

Figure 16. Comparison of H_2 production costs assuming 1MW electrolyzer. Capital costs for Steam Methane Reforming (SMR), Alkaline Electrolysis (Alk), Proton Exchange Membrane Electrolysis (PEM), Anion Exchange Membrane Electrolysis (AEM), Solid Oxide Electrolyzer Cell (SOEC) are reported in published literature.[27] Costs for Direct Electrolysis (DE), Anion Exchange Membrane Electrolysis (AEM) and Cation Exchange Membrane Electrolysis (CEM) using Pt and MnMo/Ti anodes are estimated based on results conducted in this study. Assumptions underlying these calculations are noted in Table 10-11.

Figure 17. Estimated revenue and costs for using electrolysis routes assuming that 1MW electrolyzer is used. Assumptions underlying this calculation are noted in Table 12-15.

Figure 18. Schematic representation of the Direct Electrolysis (DE) process with MnMO/Ti electrode.

Figure 19. Process flow diagram and phase boundary for brine electrolysis system. The mass balance calculations for this life cycle inventory are based on the production

of 1 kg of hydrochloric acid and are determined using experimental data. These numbers were then scaled up to 1,000 kg for the Life Cycle Impact Assessment.

Figure 20. Life cycle impacts on greenhouse gas emissions (GHG), energy use and water usage using MnMo/Ti anode and stainless steel cathode for direct electrosynthesis (DE) of brine, with a production scale of 1 metric ton of hydrochloric acid.

LIST OF TABLES

LIST OF ABBREVIATION

Abbreviation	Definition
BMED	Bipolar-Membrane Electrodialysis
DE	Direct Electrosynthesis
AEM	Anion Exchange Membrane
CEM	Cation Exchange Membrane
MnMO/Ti	Manganese-Molybdenum coated Titanium
MSF	Multi-Stage Flash
MED	Multi-Effect Distillation
RO	Reverse Osmosis
PW	Pure Water
BR	Brine
SW-RO	Sea Water-Reverse Osmosis
NF	Nanofiltration
ED	Electrodialysis
EDI	Electrodeionization
EDR	Electrodialysis Reversal
SEM	Scanning Electron Microscopy
EDS	Energy Dispersive X-ray Spectroscopy
CER	Chlorine Evolution Reaction
OER	Oxygen Evolution Reaction
PEM	Proton Exchange Membrane Electrolyzer
AEM	Anion Exchange Membrane Electrolyzer
SOEC	Solid Oxide Electrolyzer Cell
LCA	Life Cycle Assessment
LCI	Life Cycle Inventory
TEA	Techno Economic Analysis

CHAPTER 1

Introduction to Brine Electrolysis for Sustainable Hydrogen Production

The global energy industry is moving away from the reliance on fossil fuels towards cleaner, carbon-free alternatives, with a goal of achieving carbon Net-Zero by 2050.[1] In this context, utilizing hydrogen and renewable energy is one of the most effective ways to mitigate greenhouse gas emissions and corresponding global warming. Despite being widely regarded as clean sources of energy, renewable energy sources such as solar, wind, and hydro power face an issue of intermittency.[2] This means that the output of energy can fluctuate depending on factors such as weather conditions and seasonal changes, resulting in an inconsistency with energy demand.

To address this issue, energy storage systems are essential to preserve the surplus electricity generated during periods of excess wind or solar energy and release it when needed. However, conventional batteries can only store energy for a limited period, typically one to five days,[3] which heavily impede its application in industry with a large scale. In contrast, hydrogen can serve as an ideal energy carrier because it has the potential for longer-term storage, even at a seasonal scale.[3] This approach will enhance the stability and adaptability of the power system and aid in achieving low carbon H_2 conversions. Furthermore, hydrogen can be a low-carbon alternative fuel in various industries, including transportation (such as trucks and aircraft), commerce, industry, and housing, where decarbonization is challenging.[4] Thus, green hydrogen produced through water splitting with renewable energy sources is widely considered a crucial component in the transition to clean energy.

In recent years, there has been a growing interest in the use of hydrogen as a clean and renewable energy source, as it has the potential to replace fossil fuels and reduce greenhouse gas emissions. However, the production of hydrogen is still mainly dependent on fossil fuels, which undermines its environmental benefits. One promising solution to this challenge is the use of brine.

Due to the growing scarcity of water resources in many parts of the world and the increasing demand for fresh water, desalination technologies have become more popular. This has been driven by population growth, urbanization, and industrialization, resulting in a rise in global demand for desalinated water.[5] However, one of the major challenges associated with desalination is the disposal of the brine byproduct generated during the process. Brine is a concentrated salt solution that remains after desalination, and it contains high levels of salt and other metals.[6] The high salinity of the brine can be harmful to marine life, and it often contains other contaminants.[7]

From this perspective, rather than disposing of brine into the ocean, there is a need to produce valuable products using electrolysis.[8] This study aims to conduct experiments on brine electrolysis by designing an anode that limits the evolution of chlorine gas and assessing its production output (H_2, O_2, base, and acid), energy consumption, and economic viability. Specifically, the study will focus on a process that involves coupling brine with direct electrosynthesis (DE), using an anion exchange membrane (AEM) and cation exchange membrane (CEM) electrolysis.

1.1 Brines for electrochemical H_2 production

The increasing demand for fresh water, coupled with the growing scarcity of water resources in many regions of the world, has led to an increased interest in desalination technologies. Desalination is seen as a potential solution to address the water crisis in arid and water-stressed regions, especially in coastal areas where seawater is abundant. The global demand for desalinated water has been steadily increasing in recent years, driven by population growth, industrialization, and urbanization. Current estimates indicate that 40% of the world's population is experiencing acute water scarcity, which is expected to increase to 60% by 2025.[9] Additionally, approximately 4 billion people, or 66% of the global population, currently face severe water scarcity for at least one month per year.[10]

One of the biggest challenges associated with desalination is the disposal of the brine byproduct generated during the process. Brine is the highly concentrated salt solution that remains after the desalination process, containing high levels of salt and other metals.[6] As shown in **Figure 1**, brine is generated through the desalination of seawater, as shown in left side.[8] The bottom quadrant illustrates that salt brines are created both through the desalination of brackish groundwater and via salt mining. Finally, the top-right quadrant of the figure shows that brine is also produced as a by-product of effluent-treated industrial wastewater.[8]

Disposing of brine is a major environmental concern, as it can have a negative impact on marine ecosystems if not properly treated and discharged. Brine disposal can also

pose a significant economic challenge, as the cost of disposing of brine can be high, especially in areas with limited space or poor infrastructure. The challenge of brine disposal is becoming increasingly urgent as desalination plants continue to proliferate around the world. According to the International Desalination Association, the global desalination capacity reached 95 million cubic meters per day in 2019,[11] and this is expected to grow to double by 2030. This growth in desalination capacity will also lead to an increase in the amount of brine generated, exacerbating the brine disposal problem.

To address the brine problem, there have been efforts to develop new technologies and strategies for brine disposal and management. One approach is to use innovative treatment methods, such as membrane-based technologies, to extract valuable minerals from brine and reduce its volume. Another approach is to explore alternative uses for brine, such as in aquaculture or agriculture, which can help to offset the cost of brine disposal and reduce the environmental impact of brine discharge. In this thesis, approaches to convert low-value brines to H_2 and multiple co-products such as NaOH and HCl using electricity will be developed.

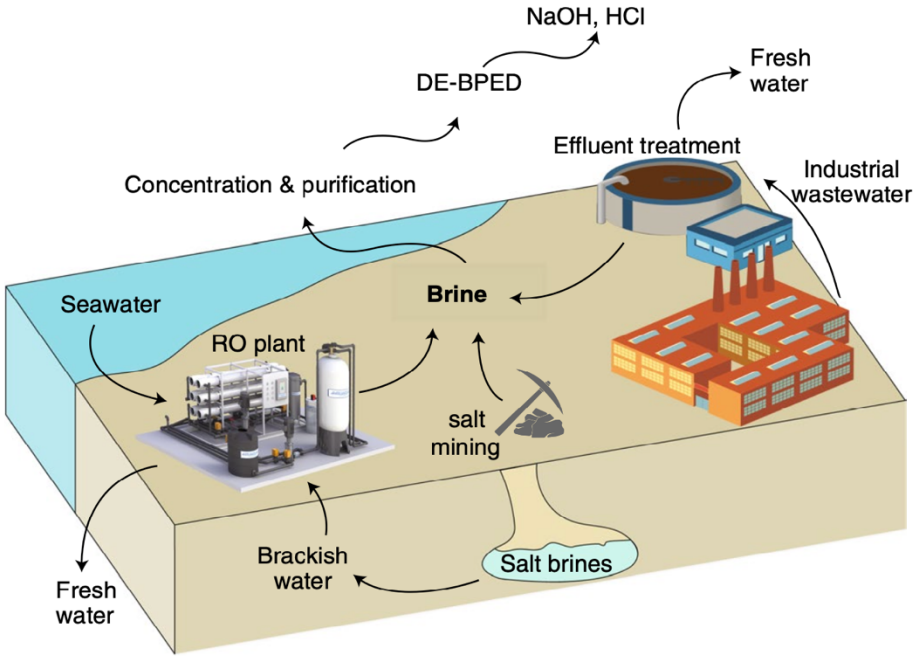

Figure 1. Schematic illustration of different sources of brine for the DE-BMED process.[8]

1.1.1 Global State of Desalination

According to **Figure 2 (a)**, there are 15,906 operational desalination plants worldwide, with a total capacity of approximately 95.37 million m^3/day (34.81 billion m^3/year), which accounts for 81% and 93% of the total number and capacity of all desalination plants ever constructed, respectively.[11] Early desalination plants predominantly utilized thermal technologies and were in water-scarce regions, especially in the Middle East where oil reserves were abundant.[11] Prior to the 1980s, thermal technologies such as multi-stage flash (MSF) and multi-effect distillation (MED) dominated the desalination industry, accounting for 84% of global desalinated water production.[11] However, the rise of membrane technologies, particularly reverse osmosis (RO), gradually shifted the dominance away from

thermal technologies.[11] In 2000, the production volumes of desalinated water using thermal technologies (primarily MSF) and RO were nearly equal at 11.6 million m^3/day and 11.4 million m^3/day, respectively, accounting for 93% of the total volume of desalinated water produced, as shown in **Figure 2 (b)**.[11] Since 2000, RO plants have experienced an exponential increase in both number and capacity, whereas thermal technologies have only experienced marginal growth, as depicted in **Figure 2 (b)**.[11] Currently, the production of desalinated water using RO stands at 65.5 million m^3/day, accounting for 69% of the total volume of desalinated water produced.[11]

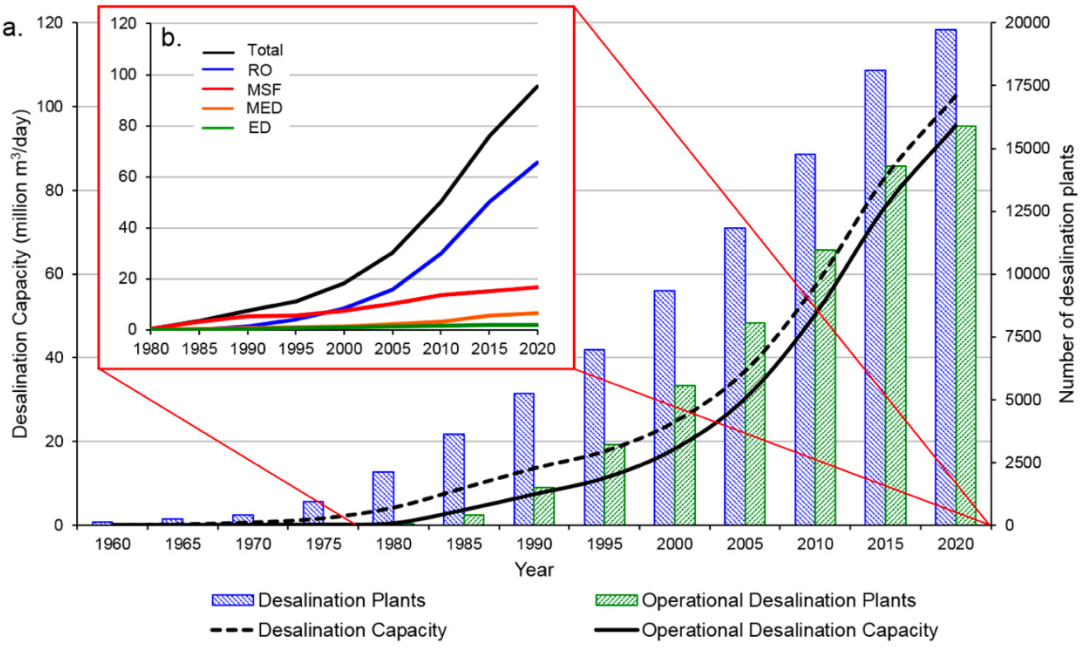

Figure 2. Trends in global desalination by (a) number and capacity of total and operational desalination facilities and (b) operational capacity by desalination technology.[11]

As illustrated in **Figure 3**, desalination facilities with a capacity of over 1,000 m^3/day are distributed across various regions, including Europe, North Africa, the Middle East, the United States, China, and Australia. However, South America and Africa have relatively fewer desalination facilities, which are primarily designed to produce desalinated water for the industrial sector.[11] Desalination plants are mainly located on or near coastlines, and coastal plants tend to be larger than inland plants.[11] Plants that produce municipal water are found worldwide, but they are particularly prevalent in the Middle East and North Africa.[11] In contrast, a larger proportion of desalination plants producing non-municipal water are located in North America, Western Europe, and East Asia and the Pacific.[11] These plants primarily generate water for industrial and power applications, which also make up a substantial portion of the market share, as shown in **Figure 3**.[11]

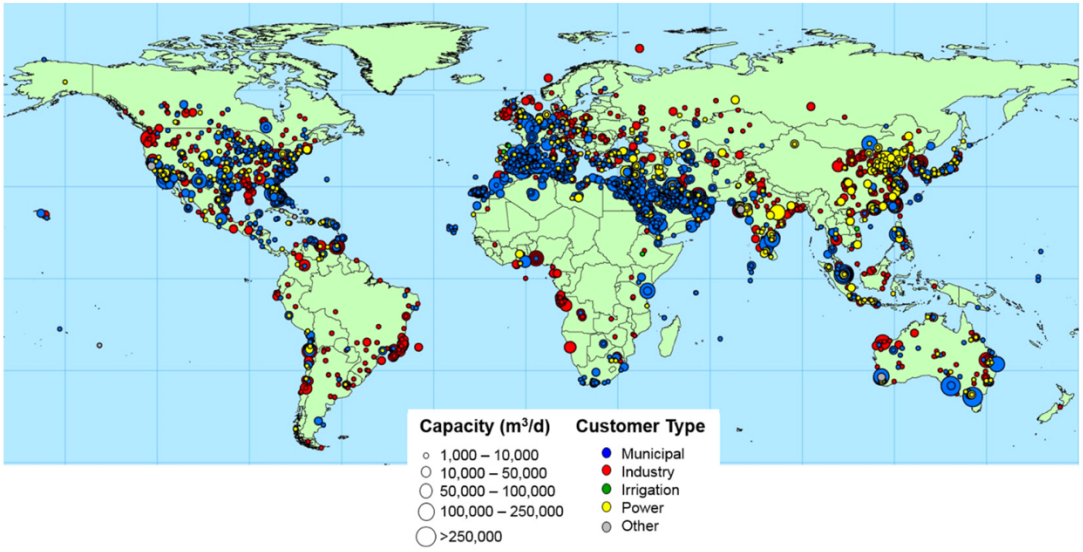

Figure 3. Global distribution of operational desalination facilities and capacities (>1000 m^3/day) by sector user of produced water.[11]

1.1.2 Brine Production

The efficiency of water recovery during desalination depends on the type of technology used and the quality of the feedwater.[11] Thus, it is important to consider both factors when estimating brine production. **Table 1** shows the water recovery ratios for various feedwater-technology combinations. The recovery ratio increases as feedwater quality improves (i.e., salinity decreases). Pure water (PW) has the highest recovery ratio, whereas brine (BR) has the lowest. The type of feedwater used also plays a significant role in determining the recovery ratio associated with a particular technology.[11] For instance, sea water-reverse osmosis (SW-RO) has a substantially lower recovery ratio (0.42) than brackish-reverse osmosis (0.65) and river- reverse osmosis (0.85). Similarly, brackish-nanofiltration (0.83) is more efficient than sea water-nanofiltration (0.69). Different desalination technologies are also associated with different recovery ratios, with thermal technologies (e.g., MSF, MED) typically having lower ratios than membrane technologies (e.g., reverse osmosis, nanofiltration). MSF has a recovery ratio that is approximately half that of RO across all feedwater types. Additionally, the water recovery ratio of other membrane technologies such as nanofiltration (NF), electrodialysis (ED), electrodeionization (EDI), and electrodialysis reversal (EDR) is substantially higher than that of RO for all feedwater types.[11]

Table 1. Recovery ratios of various combinations of feedwater and technologies for producing desalinated water.[11]

Feedwater type	Technology							
	RO	MSF	MED	NF	ED	EDI	EDR	Other
Seawater (SW)	0.42	0.22	0.25	0.69	0.86	0.90		0.40

Brackish (BW)	0.65	0.33	0.34	0.83	0.90	0.97	0.90	0.60
River (RW)	0.81		0.35	0.86	0.90	0.97	0.96	0.60
Pure (PW)[a]	0.86	0.35		0.89	0.90	0.97	0.96	0.60
Brine (BR)	0.19	0.09	0.12		0.85			0.40
Wastewater (WW)[b]	0.65	0.33	0.34	0.83	0.90	0.97		0.60

[a] PW refers to water of a high base quality (low salinity), but that is desalinated primarily for industrial applications requiring very low salinity water (e.g., food processing, pharmaceutical manufacturing).
[b] WW refers to reject water from municipal and industrial sources undergoing desalination in specific WW desalination facilities.

Brine is the highly concentrated saltwater solution that is generated as a byproduct of desalination operations. The global brine production rate of 141.5 million m^3/day, or 51.7 billion m^3/year, is approximately 50% greater than the total volume of desalinated water produced globally (**Table 2**).[11] The majority of brine production occurs in the Middle East and North Africa, which accounts for 70.3% of global brine production, with a daily brine production of almost 100 million m^3.[11] This indicates that desalination plants in this region operate at a very low average water recovery ratio of 0.25, meaning that a significant amount of feedwater is being discharged as brine.[11] In other regions, including East Asia and Pacific, Western Europe, and North America, brine production is lower than the amount of desalinated water produced, indicating that recovery ratios are generally high. In case of North America, an average recovery ratio is 0.75.[11] In other geographical regions, brine production is approximately equivalent to desalinated water production, with a recovery ratio of 0.5.[11]

Table 2. Global brine production and distribution by region, income level and sector use.[11]

	Brine production	
	(million m^3/day)	(%)
Global	141.5	100
Geographic region		

Middle East & North Africa	99.4	70.3
East Asia & Pacific	14.9	10.5
North America	5.6	3.9
Western Europe	8.4	5.9
Latin America & Caribbean	5.6	3.9
Southern Asia	3.7	2.6
Eastern Europe & Central Asia	2.5	1.8
Sub-Saharan Africa	1.5	1.0
Income level		
High	110.2	77.9
Upper middle	20.7	14.6
Lower middle	10.5	7.4
Low	0.03	0.0
Sector use		
Municipal	106.5	75.2
Industry	27.4	19.3
Power stations	5.8	4.1
Irrigation	1.1	0.8
Military	0.5	0.3
Other	0.3	0.2

The location of brine production facilities impacts the viability of various methods for its disposal.[12] Desalination plants near coastlines often release untreated brine into saline water bodies such as oceans and seas.[12] The majority of countries producing large amounts of brine (>1 million m^3/day) in coastal areas are located in the Middle East and North Africa (e.g., UAE, Saudi Arabia), South-East Asia (China, India), the USA, and Australia (**Figure 4 (a)**). The volume of brine produced in many of these countries, particularly in the Middle East, greatly exceeds 1 million m^3/day, with the four largest brine producers in the region (UAE, Saudi Arabia, Qatar, Kuwait) accounting for 72.2 million m^3/day within 10 km of the coastline.[11]

Although disposal of brines in saline surface water bodies raises environmental concerns, this method is cost-effective.[12] However, inland desalination plants, which produce a smaller but significant amount of brine, often do not have this option

available. Approximately 22 million m^3/day of brine is produced over a distance of more than 50 km from the nearest coastline. Despite the large volume of inland brine produced, very few economically viable and environmentally safe options exist for managing it.[12] Inland brine production is a significant issue in 64 countries across the globe, with brine production exceeding 10,000 m^3/day (**Figure 4 (b)**). While coastal brine production is primarily concentrated in the Middle East, inland brine production is a problem in other areas such as China (3.82 million m^3/day), the USA (2.42 million m^3/day), and Spain (1.01 million m^3/day).[11]

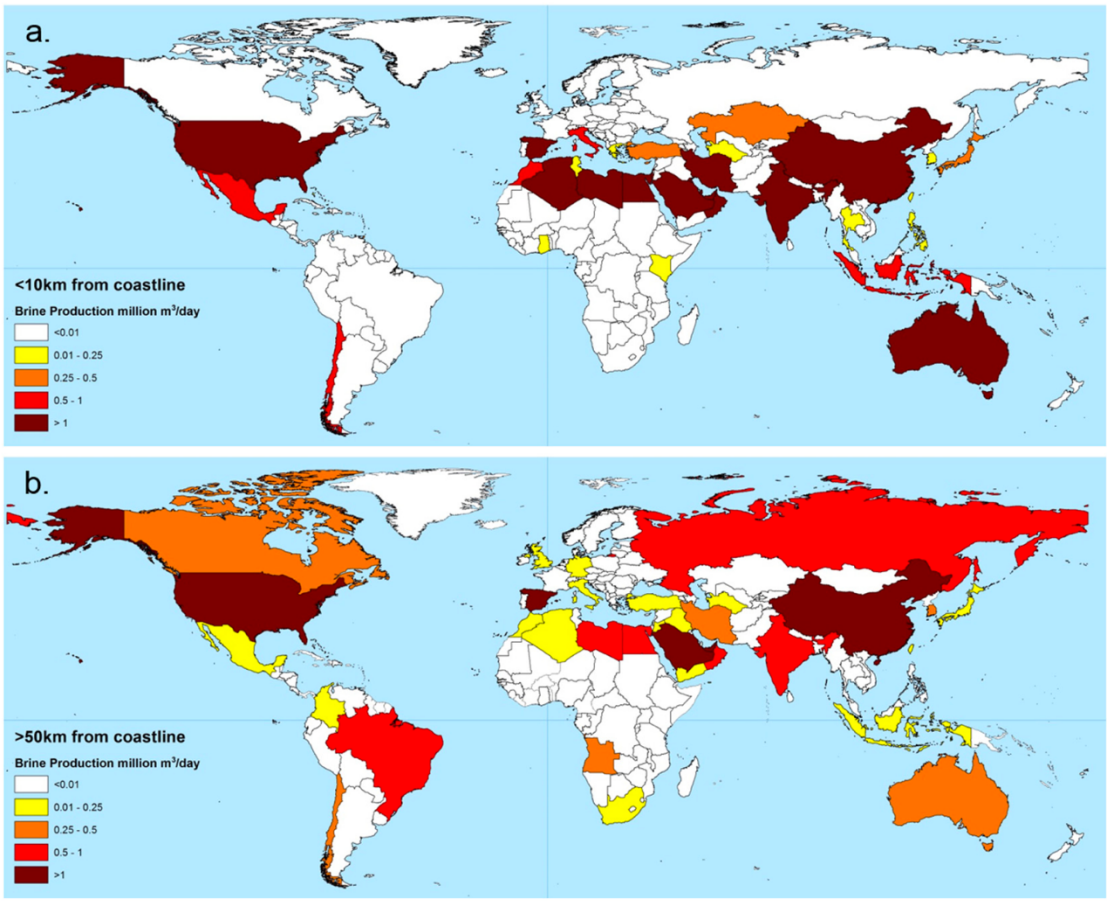

Figure 4. Volume of brine produced per country at a distance of a) <10 km and b) >50 km from the coastline.[11]

1.2 Brine Electrolysis System

Recently, there has been a growing interest in the use of electrochemical methods to produce hydrogen from brine, as well as base and acid. A variety of cell configurations are developed to improve performances, including bipolar-membrane electrodialysis (BMED), direct electrosynthesis (DE), anion exchange membrane (AEM), and cation exchange membrane (CEM) systems. More features of each configuration are detailed described as follows. (**Figure 5**)

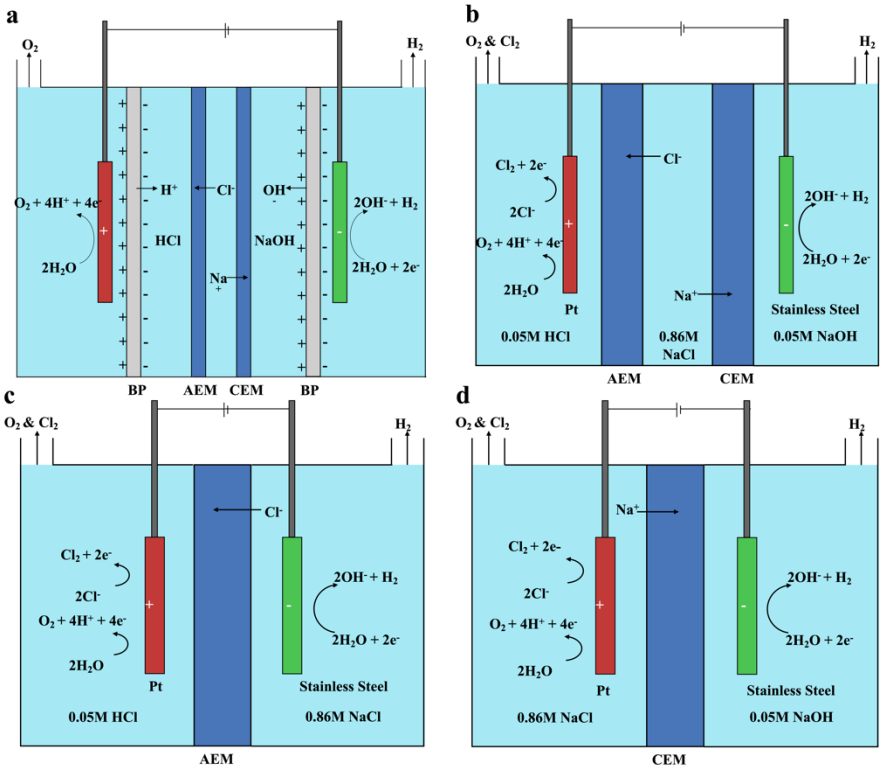

Figure 5. Schematic drawings of brine electrolysis systems. (a) Bipolar membrane electrodialysis (BMED) (b) Direct electrosynthesis (DE) (c) Anion exchange membrane electrolysis (AEM) (d) Cation exchange membrane electrolysis (CEM).

1.2.1 Bipolar-Membrane Electrodialysis (BMED)

One approach that has been explored is the use of Bipolar-Membrane Electrodialysis (BMED), which utilizes four membranes. A bipolar membrane consists of two layers, namely an anion exchange layer and a cation exchange layer (**Figure 5 (a)**). This setup enhances the separation of water into protons and hydroxide ions. Furthermore, the anion-exchange layer of the bipolar membrane is designed to selectively allow the transport of anions, such as chloride ions, across the membrane. However, the cation-exchange layer is designed to prevent the transport of anions such as chloride ions. As a result, the formation of chlorine gas in the anode can be prevented (as shown in **Figure 5 (a)**). Equation (1) indicates that oxygen gas is produced at the anode as a result of suppression of chlorine oxidation reaction. Meanwhile, Equation (2) demonstrates that two electrons are transferred to the proton at the cathode, resulting in H_2 production. The electrolysis of water produces protons and hydroxide ions according to Equation (3). Additionally, NaOH and HCl can be produced by the reaction between NaCl and water, as shown in Equation (4). Although this configuration can suppress chlorine gas production, some problems have not been addressed to support large-scale industrial applications, such as materials, operating costs, and complex design.[8]

$$\text{Anode: } H_2O \rightarrow \frac{1}{2}O_2 + 2H^+ + 2e^- \quad (1)$$

$$\text{Cathode: } 2H_2O + 2e^- \rightarrow H_2 + 2OH^- \quad (2)$$

$$\text{BP: } 2H_2O \rightarrow 2H^+ + 2OH^- \quad (3)$$

$$\text{Overall: } 2NaCl + 2H_2O \rightarrow 2HCl + 2NaOH \ (1.23V @ 25℃) \quad (4)$$

1.2.2 Direct Electrosynthesis (DE)

In contrast to BMED, Direct Electrosynthesis (DE) utilizes only cation and anion membranes, resulting in a simplified configuration with lower energy consumption[8] (**Figure 5 (b)**). However, when brine electrolysis is applied, Cl_2 is generated along with O_2 at the anode (Equation 5, side reaction). The corrosivity and toxicity of Cl_2 makes DE system unsuitable for practical use. Moreover, the anode materials currently available tend to promote chlorine evolution instead of O_2.[8] These challenges motivate the development of anodes that inhibit Cl_2 production. In this context, the relevant reactions are discussed below.

Equation (5) illustrates the water splitting reaction at the anode to produce O_2, as well as protons. In the presence of an electric field, Cl^- ions migrate to the anode chamber and react with the formed protons, resulting in HCl production. H_2 and hydroxide ions are produced at the cathode (Equation 6). The hydroxide ions then react with Na^+ ions to form NaOH (Equation 7).

$$\text{Anode: } H_2O \rightarrow \frac{1}{2}O_2 + 2H^+ + 2e^- \quad (5)$$

$$\text{Side reaction at anode: } Cl^- + 2e^- \rightarrow Cl_2$$

$$\text{Cathode: } 2H_2O + 2e^- \rightarrow H_2 + 2OH^- \quad (6)$$

$$\text{Overall: } 2NaCl + 2H_2O \rightarrow 2HCl + 2NaOH \ \ (2.06V\ @\ 25°C) \quad (7)$$

1.2.3 Anion and Cation Exchange Membrane System (AEM&CEM)

As shown in **Figures 5 (c) & 5 (d)**, The Anion Exchange Membrane (AEM) and Cation Exchange Membrane (CEM) systems both use only one membrane, as compared to the two used in Direct Electrosynthesis (DE). In the AEM system, NaCl solution is placed in the cathode chamber using the anion exchange membrane and the anion Cl^- anion is transported to the anode chamber to produce HCl, as shown in Equations (8) and (9). In the cathode chamber, OH^- ions are created through water splitting and combine with Na^+ ions to produce NaOH, as seen in Equations (10) and (11). Similarly, the CEM system uses a cation exchange membrane to produce HCl and NaOH, following the same principle as the AEM system. Like the aforementioned DE system, both the AEM and CEM systems simultaneously produce O_2 and Cl_2 at the anode.

$$\text{Anode: } 2H_2O \rightarrow O_2 + 4H^+ + 4e^- \quad (8)$$

$$4H^+ + 4Cl^- \rightarrow 4HCl \quad (9)$$

$$\text{Cathode: } 2H_2O + 2e^- \rightarrow H_2 + 2OH^- \quad (10)$$

$$2OH^- + 2Na^+ \rightarrow 2NaOH \quad (11)$$

Table 3. Selected electrochemical studies for the production of bases and acids

System	Feed concentrat (M)	Current density (mA/cm^2)	Current efficiency (%)	Max.Base concentration (M)	Max. Acid Concentration (M)	Energy consumption (kWh/kg)	Suppressing Cl_2	Produced H_2 (Mol)	Ref
DE	NaCl 0.86	90	Acid 20 Base 36	NaOH 0.37	HCl 0.2	NaOH 3.6	Yes (Anode: Ti coated with MnMo)	0.005	This work
DE	NaCl 0.86	90	Acid 11 Base 28	NaOH 0.63	HCl 0.25	NaOH 2.2	No (Anode: Pt)	0.017	This work
DE	NaCl 0.6	25	Acid 65 Base 88	NaOH 0.22	HCl 0.29	n.a	Yes (Anode: Ti coated with MnMo)	n.a	13
DE	K_2SO_4 0.5	10	n.a	KOH (-)	H_2SO_4 (-)	n.a	n.a	n.a	14
B M E D	NaCl 1	100	n.a	NaOH 3.65	HCl (-)	NaOH 22.6	-	n.a	15

B M E D	Waste water	40	Acid 55.2 Base 50.2	NaOH 1.56	H_2SO_4 0.97	NaOH 3.98	-	n.a	16
B M E D	NaCl 0.5	50	41-59	NaOH 3.4	HCl 2.3	NaOH 1.5-1.9	-	n.a	17
B M E D	NaCl 1	100	n.a	NaOH 3.6	HCl 3.3	HCl 43.5	-	n.a	18
B M E D	NaCl 1.3	3.67V	50-53	NaOH 1.75	HCl 1.75	n.a	-	n.a	19
B M E D	NaCl 1.7-3.4	30-40	55-58	NaOH 2	HCl 2	NaOH 1.7-3.6	-	n.a	20
Mem Brane less	Sea water	1V	n.a	NaOH	HCl	n.a	No (Platinized carb foam electrod	n.a	21

As shown in **Table 3**, most of the research has been concentrated on BMED, with little information available on hydrogen production. The focus of BMED studies has been on enhancing the concentration of acid and base for commercial purposes or reducing energy consumption. Some of the methods proposed include increasing the concentration of NaOH through the addition of an evaporation process[15] and determining the optimal volume ratio of acid, base, and salt used[17]. However, there have been limited studies on Direct Electrosynthesis (DE) to prevent the generation of Cl_2. In 2016, Lin and co-workers successfully inhibited Cl_2 generation by using a Mn0.84Mo0.16O0.23 coated titanium electrode in DE, but the resulting NaOH concentration was low, and energy consumption data were not provided.[13] Recently, Zhu and co-workers produced KOH and H_2SO_4 using DE, but NaCl solution was not utilized.[14] Additionally, in 2022, Palash and co-workers successfully produced NaOH and HCl without the use of a membrane and generated $MgOH_2$, which can be used as a feedstock for cement production using NaOH. However, there is no information available on the concentration of NaOH, HCl, and H_2 produced, or whether the formation of Cl_2 was inhibited.[21]

In this study, an electrochemical approach is developed for the continuous production of H_2, O_2, NaOH, and HCl from brine. This approach utilizes three systems: direct electrosynthesis (DE), anion exchange membrane (AEM), and cation exchange membrane (CEM) systems. DE is an energy-efficient technique that reduces energy consumption by reducing the number of membranes from four to two compared to bipolar-membrane electrodialysis (BMED).[8] AEM and CEM systems utilize anion and cation exchange membranes, respectively, to produce H_2, O_2, NaOH, and HCl, with a simplified configuration by reducing the number of membranes from two to one compared to DE. It is worth noting that manganese-molybdenum oxide coated titanium anode was developed for selective oxygen evolution in brine electrolysis, which helps to inhibit chlorine gas production during the electrolysis process. Also, the feasibility and economics of brine management potential using DE, AEM, and CEM systems are discussed. Finally, a life cycle analysis (LCA) was conducted to evaluate the environmental impacts of the DE-MnMo/Ti system.

CHAPTER 2

EXPERIMENTAL APPROACH FOR PRODUCING H_2, ACIDS, AND BASES VIA BRINE ELECTROLYSIS

In this section, the experimental approach for producing H_2, HCl, and NaOH via brine electrolysis are discussed.

2.1 Materials used in brine electrolysis studies

The synthetic brines used in this study were prepared using sodium chloride (NaCl, ≥ 99%, Sigma-Aldrich). Acid and base adjustments were made using hydrochloric acid (HCl, 12.1 N, Fisher chemical) and sodium hydroxide (NaOH, Lab grade, Fisher bioreagents). The catalysts were synthesized using manganese sulfate ($MnSO_4$, ≥ 98%, Chemworld), sodium molybdate dihydrate ($Na_2MoO_42H_2O$, ≥ 99.5%, Sigma-Aldrich), ascorbic acid ($C_6H_8O_6$, 100%, Cole-Parmer), and potassium iodide (KI, ≥99%, Sigma-Aldrich). Deionized water (18.2 MΩ·cm, Millipore) was used throughout the experiments.

2.2 Experimental Approach

Experimental studies are conducted to investigate the feasibility of co-producing O_2, H_2, HCl, and NaOH using DE, AEM, and CEM systems using a model brine solution with a concentration of 0.86 M NaCl. **Figure 6** is a schematic representation of this experimental approach. Alternating Pt and MnMo/Ti anode electrodes were tested on three systems. The cell used a batch system, with anolyte consisting of HCl solution (0.05 M, 50 ml), catholyte consisting of NaOH solution (0.05 M, 50 ml), and the middle solution consisting of NaCl solution (0.86 M, 50 ml). The aqueous solutions were injected into the chamber using a peristaltic pump. 50 ml of the solution was

injected each time. During the experiment, a current density of 90 mA/cm^2 was applied using a galvanostat for 5 hours.

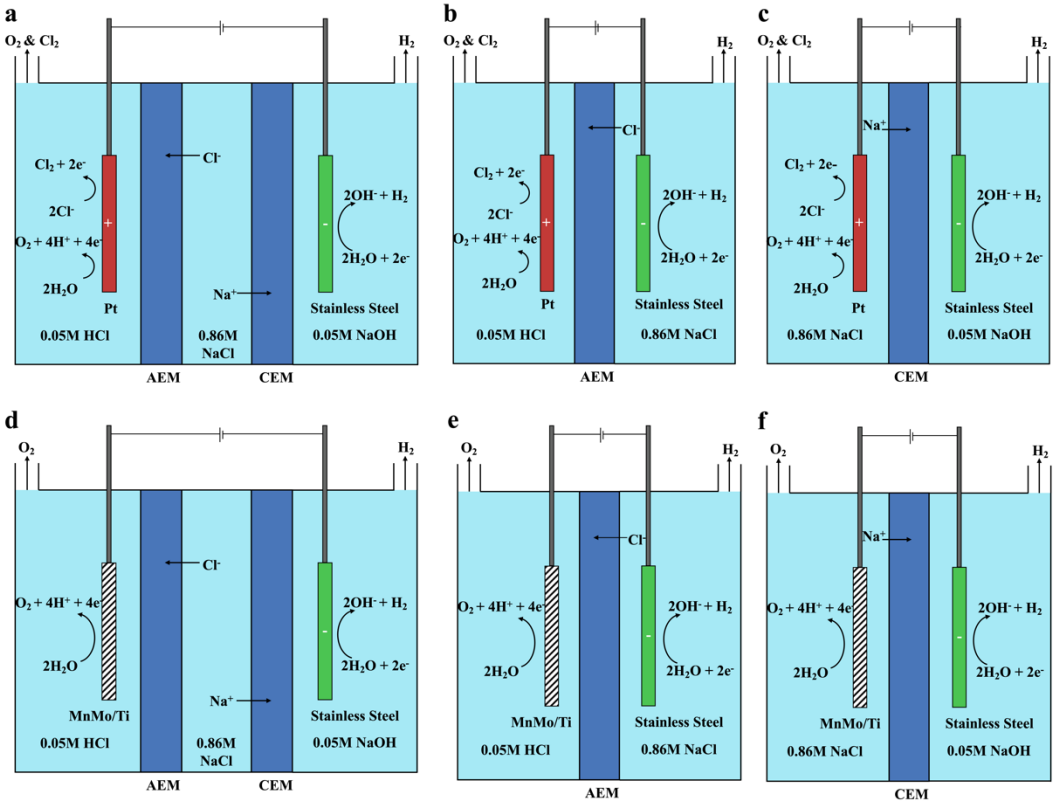

Figure 6. Schematic overview of the experimental setup. (a) Direct electrosynthesis (DE) using Pt anode, (b) Anion exchange membrane electrolysis (AEM) using Pt anode, (c) Cation exchange membrane electrolysis (CEM) using Pt anode, (d) Direct electrosynthesis (DE) using MnMo/Ti anode, (e) Anion exchange membrane electrolysis (AEM) using MnMo/Ti anode, and (f) Cation exchange membrane electrolysis (CEM) using MnMo/Ti anode.

2.3 Electrochemical Cell for Brine Electrolysis

A customized electrochemical cell was designed for brine electrolysis. The design of this cell is shown in **Figure 7**. The cell has two end plates and three compartments with outer dimensions of 10 × 10 × 2 cm, totaling a volume of 72 cm^3. It was built using a 3D printer with polyethylene material that can withstand both acidic and basic conditions. The anode compartment has openings for the anode, gas outlet, and

reference electrode. The cathode compartment has openings for the cathode (made of stainless steel, 26 × 24 mm) and a gas outlet. The cell also has six gaskets made of EPDM rubber with a thickness of 1.6mm, and the dimension of each gasket is 10 × 10 cm. Two gaskets are placed between the anode compartment and the middle compartment to secure the Anion Exchange Membrane (Fumasep FAM) and prevent hydrogen and oxygen gas from leaking. The size of the used Anion Exchange Memebrane (AEM) and Cation Exchange Membrane (CEM, Nafion 117) is 10 × 10 cm. The two end plates provide support to the three compartments, and 12 holes (diameter 5 mm) are made to join the 5 compartments. 12 clamping bolts are also inserted.

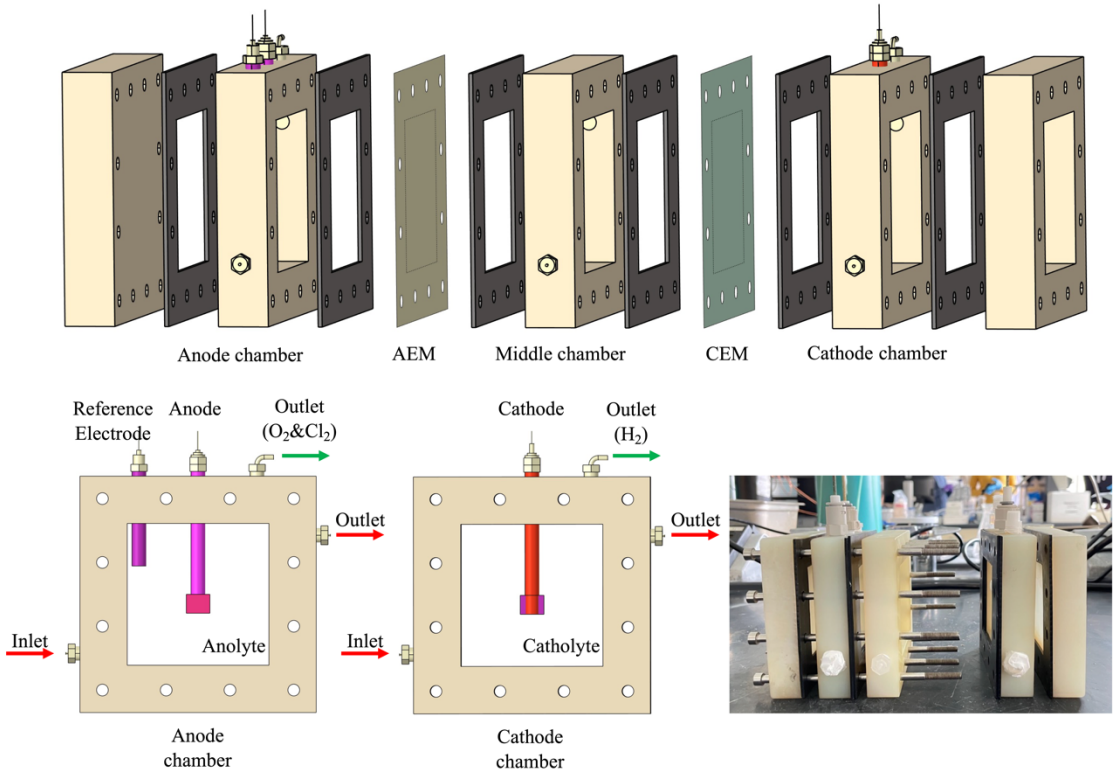

Figure 7. Customized cell for brine electrolysis. This cell is composed of three chambers and two end plates.

2.4 Fabrication of Manganese-Molybdenum Oxide Anode

An anodic deposition strategy was utilized to fabricate MnMo coated titanium anode. In detail, a mixture of 0.4M MnSO4 and 0.003M Na_2MoO_4 was used as the electrolyte. The anode was made of titanium with dimensions of 10 × 10 × 1mm, while the cathode was made of platinum with dimensions of 15 × 15 × 1mm. A constant current density of 60mA/cm^2 was applied at a temperature of 90°C for 1 hour.[22] By employing H-type cells, a suitable separation is ensured between the anode and the cathode. When a potential is applied, manganese and molybdenum ions migrate towards the anode, enabling their deposition onto the titanium surface.

After the reaction, the manganese and molybdenum were found to have been anodically deposited on the titanium surface. The morphology of the materials was studied using Scanning Electron Microscopy (SEM), specifically using the Zeiss LEO 1550 FESEM instrument. Scanning electron microscopy (SEM) images (**Figure 8 (a) and 8 (b)**) show the formation of titanium and MnMo coated titanium. Also, energy dispersive X-ray spectroscopy (EDS) mappings shows a strong signal of Mn and Mo (**Figure 8 (c)**).

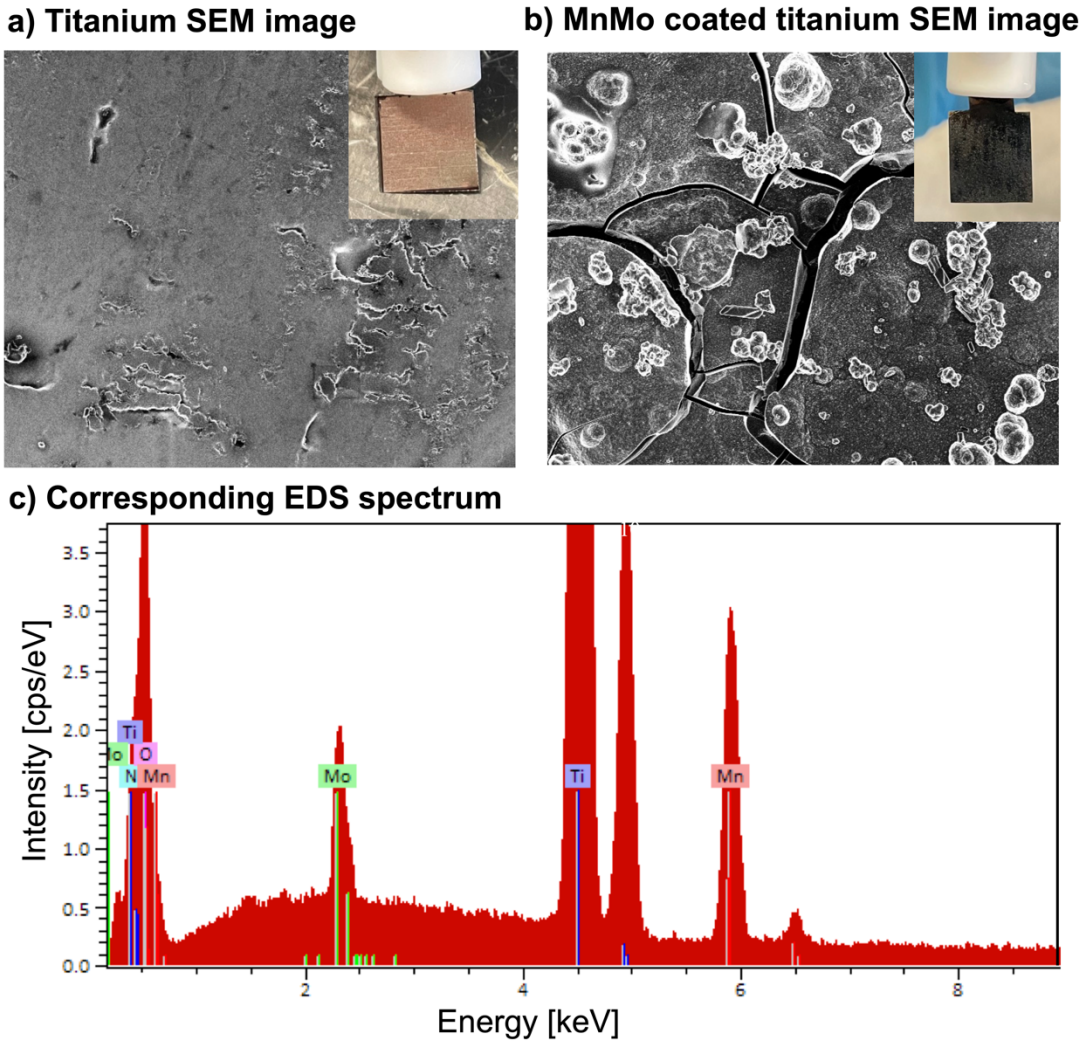

Figure 8. SEM images of (a) Titanium matrix and (b) MnMo coated titanium (MnMo/Ti). (c) The corresponding EDS spectrum of MnMo/Ti.

2.5 Analysis of the products from brine electrolysis

2.5.1 Determination of HCl and NaOH Concentrations

The concentrations of HCl and NaOH were determined by titration using solutions of 0.5M HCl and 0.5M NaOH. The volume of hydrogen produced at the cathode was measured using a gas flow meter (OMEGA FMA1808A).

2.5.2 Determination of Cl_2 Concentrations

The concentration of Cl_2 produced in the anode was measured through iodometric titration. The gas produced in the anode was passed through a solution of KI with a concentration of 25g/500 ml, and as per Equation (12), the chlorine gas reacted with I^- to produce I_2 (**Figure 9 (a)**). As Cl_2 reacts with KI solution, the transparent KI solution changes to a reddish brown (**Figure 9 (b)**). The concentration of I_2 is determined through iodometric titration using ascorbic acid ($C_6H_8O_6$, 0.0008M) and starch as the indicator (Equation 13). When the titration reaches the endpoint, the ascorbic acid turns from transparent to purple, indicating that the I_2 has been fully reacted (**Figure 10**). The concentration of I_2 can be calculated using Equation (14). With the concentration of I_2 known, the concentration of Cl_2 can also be calculated. The volume of Cl_2 can be determined by the volume of KI solution (500ml) used in the experiment. Note that the concentration of Cl_2 is below 10 ppm, the iodometric titration method may not be reliable. In this case, a measurement kit is used for chlorine measurement instead (chemworld QCTK1120-Z).

$$Cl_2 + 2I^- \rightarrow 2Cl^- + I_2 \quad (12)^{23}$$

$$C_6H_8O_6 + I_2 \rightarrow C_6H_6O_6 + 2I^- + 2H^+ \quad (13)^{23}$$

$$M_{\text{ascorbic acid}} \times V_{\text{ascorbic acid}} = M_{\text{Iodine}} \times V_{\text{Iodine}} \quad (14)$$

(a) (b)

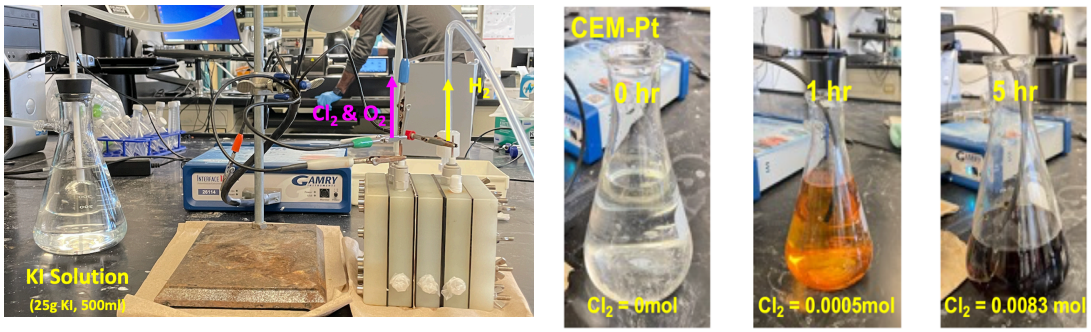

Figure 9. (a) Experimental setup of Cl_2 and O_2 gas production and quantification. (b) Color evolution of KI solution with increasing Cl_2 gas.

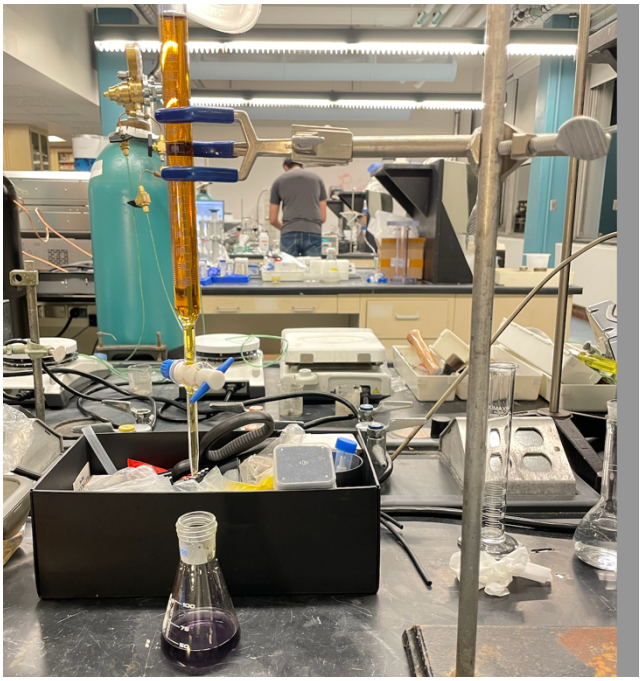

Figure 10. Ascorbic acid titration for calculating I_2 concentration quantification.

2.5.3 Oxygen Evolution Efficiency

In the experiments involving the production of chlorine gas and oxygen gas via electrolysis, it is assumed that all of the generated electrons are utilized in the production of these gases on the anode side. The amount of Cl_2 produced can be determined using iodometric titration, which also enables the calculation of the

number of electrons utilized in its production. Oxygen evolution efficiency is calculated according to Equations (15) and (16). The results are summarized in **Table 4**.

$$O_2 \text{Evolution efficiency} = 1 - Cl_2 \text{ Evolution efficiency} \quad (15)$$

$$Cl_2 \text{ Evolution efficiency} = \frac{\text{Consumed } e^- \text{ for } Cl_2}{\text{Total Coulomb}} = \frac{\text{Produced } Cl_2 \text{ [mol]} \times 2}{\text{Total Coulomb}} \quad (16)$$

Table 4. Calculated oxygen evolution efficiencies using various electrodes and membrane configurations.

Anode	System	Total Coulomb [C]	Cl_2 [mol]	Cl_2 Evolution Efficiency [%]	O_2 Evolution Efficiency [%]
Pt	DE	3,647	0.0031	16.6	83.4
Pt	AEM	3,647	0.0026	14.0	86.0
Pt	CEM	3,647	0.0083	44.0	56.0
MnMo/Ti	DE	1,621	0.0002	1.8	98.2
MnMo/Ti	AEM	1,621	0.0002	1.8	98.2
MnMo/Ti	CEM	1,621	0.0001	0.9	99.1

2.5.4 Theoretical H_2 Volume

The theoretical H_2 volume is calculated using the van der Waals relationship shown below (Equation 17).

$$\left[P + \frac{an^2}{V^2}\right] \times [V - nb] \times 1000 = n \times R \times T \quad (17)$$

- P: Pressure (bar)
- a: Hydrogen van der waals constant ($m^6 \cdot bar \cdot mol^{-2}$)
- b: Hydrogen van der waals constant ($m^3 \cdot mol^{-1}$)
- n: Mol of H_2 (mol)
- V: H_2 volume (L)
- R: Gas constant ($L \cdot bar \cdot K^{-1} \cdot mol^{-1}$)
- T: Temperature (K)

1) Determination of H_2 volume using Pt as the electrode

Table 5. H_2 volume calculation when Pt is used as an electrode

Pressure [bar]	1.01325	
a [m^6·bar·mol^{-2}]	0.24646	
b [m^3·mol^{-1}]	0.026665	
R [L·bar·K^{-1}·mol^{-1}]	0.0821	
Temperature [K]	294	Room temperature
Supplied Coulomb [C]	3,647	
Mol of e^- [mol]	0.038	Mol of e- = C/F * F=96,500
Theoretical Mol of H_2 [n]	0.0189	0.038 mol e^- supplied. (2 mol of electron for 1mol of H_2)

$$\left[1.01325 + \frac{0.24646 \times 0.0189^2}{V^2}\right] \times [V - 0.0189 \times 0.026665] \times 1000$$

$$= 0.0189 \times 0.0821 \times 294$$

$\therefore$V = 0.51L

2) Determination of H_2 volume using MnMo/Ti as the electrode

Table 6. H_2 volume calculation when MnMo/Ti is used as an electrode

Pressure [bar]	1.01325	
a [m^6·bar·mol^{-2}]	0.24646	
b [m^3·mol^{-1}]	0.026665	
R [L·bar·K^{-1}·mol^{-1}]	0.0821	
Temperature [K]	294	
Supplied Coulomb [C]	1,621	
Mol of e^- [mol]	0.017	Mol of e- = C/F * F=96,500
Theoretical mol of H_2 [n]	0.0084	0.017 mol e^- supplied. (2 mol of electron for 1mol of H_2)

$$\left[1.01325 + \frac{0.24646 \times 0.0084^2}{V^2}\right] \times [V - 0.0084 \times 0.026665] \times 1000$$

$$= 0.0084 \times 0.0821 \times 294$$

$\therefore$V = 0.22L

2.5.5 Theoretical Energy Consumption for NaOH Production

The amount of energy consumed for producing 1 g of NaOH production is calculated using Equation (18) below.

$$\frac{\text{Energy consumption [Wh]}}{\text{NaOH [g]}} = \frac{\text{U[v]} \times \text{Q[c]}}{\text{n}_{\text{NaOH}}[\text{mol}] \times \text{M} \times 3600} = \frac{\text{U[v]} \times \text{n}_{\text{e}-} \times \text{F}}{\text{n}_{\text{NaOH}}[\text{mol}] \times \text{M}[\frac{\text{g}}{\text{mol}}] \times 3600} \quad (18)$$

- U: Potential
- F: Faraday's constant (96500C/mol)
- M: Molar mass

1) Energy consumption for BMED scenario

2 mol of electrons are used to produce 2 mol of NaOH, and the potential is 1.23V.

$$\text{Anode: } H_2O \rightarrow \frac{1}{2}O^2 + 2H^+ + 2e^- \quad (1)$$

$$\text{Cathode: } 2H_2O + 2e^- \rightarrow H_2 + 2OH^- \quad (2)$$

$$\text{BP: } 2H_2O \rightarrow 2H^+ + 2OH^- \quad (3)$$

$$2NaCl + 2H_2O \rightarrow 2HCl + 2NaOH \text{ (1.23V @ 25℃)} \quad (19)[23]$$

$$\frac{\text{Energy consumption [Wh]}}{\text{NaOH [g]}} = \frac{\text{U[v]}\times\text{Q[c]}}{\text{n}_{\text{NaOH}}[\text{mol}]\times\text{M}\times3600} = \frac{\text{U[v]}\times\text{n}_{\text{e}-}\times\text{F}}{\text{n}_{\text{NaOH}}[\text{mol}]\times\text{M}\times3600} = \frac{1.23\times2\times96500}{2\times40\times3600} = 0.82\frac{\text{Wh}}{\text{g}}$$

2) Energy consumption for DE scenario

$$\text{Anode: } H_2O \rightarrow \frac{1}{2}O_2 + 2H^+ + 2e^- \quad (5)$$

$$\text{Side reactoin at anode: } Cl^- + 2e^- \rightarrow Cl_2$$

$$\text{Cathode: } 2H_2O + 2e^- \rightarrow H_2 + 2OH^- \quad (6)$$

$$2NaCl + 2H_2O \rightarrow 2HCl + 2NaOH \quad (2.06V @ 25℃) \quad (20)^{23}$$

$$\frac{\text{Energy consumption [Wh]}}{\text{NaOH [g]}} = \frac{U[v]\times Q[c]}{n_{NaOH}[mol]\times M\times 3600} = \frac{U[v]\times n_{e-}\times F}{n_{NaOH}[mol]\times M\times 3600} = \frac{2.06\times 2\times 96500}{2\times 40\times 3600} = 1.38\frac{Wh}{g}$$

3) Energy consumption for AEM scenario

$$2NaCl + 2H_2O \rightarrow 2HCl + 2NaOH \quad (2.06V @ 25℃) \quad (20)$$

$$\frac{\text{Energy consumption [Wh]}}{\text{NaOH [g]}} = \frac{U[v]\times Q[c]}{n_{NaOH}[mol]\times M\times 3600} = \frac{U[v]\times n_{e-}\times F}{n_{NaOH}[mol]\times M\times 3600} = \frac{2.06\times 2\times 96500}{2\times 40\times 3600} = 1.38\frac{Wh}{g}$$

4) Energy consumption for CEM scenario

$$2NaCl + 2H_2O \rightarrow 2HCl + 2NaOH \quad (2.06V @ 25℃) \quad (20)$$

$$\frac{\text{Energy consumption [Wh]}}{\text{NaOH [g]}} = \frac{U[v]\times Q[c]}{n_{NaOH}[mol]\times M\times 3600} = \frac{U[v]\times n_{e-}\times F}{n_{NaOH}[mol]\times M\times 3600} = \frac{2.06\times 2\times 96500}{2\times 40\times 3600} = 1.38\frac{Wh}{g}$$

2.5.6 Determination of the Current Efficiency of Base and Acid Production

The current efficiencies of base and acid productions are calculated by Equation (21).

$$\eta\,[\%] = \frac{zF(c_t V_t - c_0 V_0)}{NIt} \times 100 \qquad (21)^{15}$$

- Z: Ionic charge (1)
- F: Faraday's constant (96500C/mol)
- c_t: Acid and base concentrations at 5 hours
- c_0: Acid and base concentrations at 0
- V: Acid and base solution volume (0.05L)
- N: The number of cell units (N=3)
- I: Current (A)
- t: Experiment time (s, 5 hours)

Table 7. Current efficiencies for electrochemical of base and acid generation

Brine Electrolysis	Total Coulomb [I x t, C]	Base			Acid		
		Ct [M]	Co [M]	η [%]	Ct [M]	Co [M]	η [%]
DE-Pt	3,647	0.68	0.05	28	0.3	0.05	11
AEM-Pt	3,647	0.68	0	30	0.22	0.05	7
CEM-Pt	3,647	0.71	0.05	29	0.05	0	2
DE-MnMo/Ti	1,621	0.42	0.05	36	0.25	0.05	20
AEM-MnMo/Ti	1,621	0.29	0	29	0.22	0.05	17
CEM-MnMo/Ti	1,621	0.36	0.05	31	0.04	0	4

CHAPTER 3

CONTRASTING THE INFLUENCE OF ELECTRODES AND VARIOUS ELECTROCHEMICAL CELL CONFIGURATIONS ON THE CO-RECOVERY OF H_2, O_2, HCl, AND NaOH WITH Cl_2 SUPPRESSION

In this section, the influence of various electrodes (e.g., Pt and MnMo/Ti) and various electrochemical cell configurations (e.g., DE, AEM, and CEM) on the co-recovery of H_2, O_2, HCl, and NaOH is investigated. One of the key challenges in brine electrolysis is Cl_2 evolution. In the sections below, we discuss approaches to suppress Cl_2 evolution.

3.1 Chlorine Evolution Reaction (CER) During Brine Electrolysis

Chlorine evolution reaction (CER) is likely to occur simultaneously with oxygen evolution reaction (OER) during brine electrolysis due to the presence of chloride ions in brines (Equation 22 and 23). Although CER requires a higher potential than OER from a thermodynamic perspective, CER is kinetically more favorable than OER. This is because CER requires two electrons per mol of Cl_2, while O_2 requires four electrons.[25]

$$2Cl^- \rightarrow Cl_2 + 2e^- \quad E_o = 1.36V \tag{22}$$

$$2H_2O \rightarrow O_2 + 4H^+ + 4e^- \quad E_o = 1.23V \tag{23}$$

The selectivity of the anode material is essential in brine electrolysis for inhibiting the production of Cl_2. A reported study by Matsu in 2002 demonstrated that a manganese-molybdenum-tungsten oxide anode can suppress Cl_2 formation.[22] A recent study reported that MnOx overlayers can effectively block the diffusion of Cl^- ions, resulting in CER suppression. This study also revealed that MnOx did not participate

in the OER but acted as a Cl^- diffusion barrier.[26] In this study, a MnMo coated titanium anode is elaborately fabricated and used in all electrochemical studies. Furthermore, a comparative analysis is conducted to evaluate the impact of Direct Electrosynthesis (DE) on the evolution of Cl_2 and O_2 in contrast to Cation Exchange Membrane (CEM) and Anion Exchange Membrane (AEM) systems.

Table 8 presents the Cl_2 and O_2 ratios generated at the anode for each scenario. When Pt is used as the anode material, the Cl_2 to O_2 ratio is approximately 3:7 for both DE and AEM, while the ratio increases to 6:4 for CEM, indicating higher Cl_2 evolution. Moreover, in the case of Pt-CEM, 0.0264 mol of chloride ions remain in the anode chamber after the reaction, implying that about 40% of all chloride ions are used to produce Cl_2 gas.

Table 8. Calculated production of Cl_2 and O_2 gases at the anode

Anode	System	Cl_2 [mol]	O_2 [mol]	Ratio of Cl_2 and O_2	Total Cl^- [mol]	Cl^- in Cl_2 [mol]	Residual Cl^- [mol]
Pt	DE	0.0031	0.0079	1 : 2.5	0.046	0.0063	0.0392
Pt	AEM	0.0026	0.0081	1 : 3.1	0.046	0.0053	0.0402
Pt	CEM	0.0083	0.0053	1: 0.6	0.043	0.0166	0.0264
MnMo/Ti	DE	0.00015	0.0041	1 : 26.9	0.046	0.0003	0.0452
MnMo/Ti	AEM	0.00015	0.0041	1 : 27.2	0.046	0.0003	0.0452
MnMo/Ti	CEM	0.00008	0.0042	1 : 52.7	0.043	0.0002	0.0428

3.2 NaOH and HCl Production under Different Scenarios

The yields of NaOH and HCl were examined in various electrode and membrane configurations.

Normalization of the data is essential due to the variation in the total charge supplied to the platinum (Pt) and MnMo/Ti electrodes. The total charge supplied to the Pt electrode is 3647C, while for the MnMo/Ti electrode, it is 1621C. Consequently, it becomes apparent that the Pt cases exhibit higher base production (**Figure 11 (a)**). To ensure data comparability, normalization of the NaOH concentrations is necessary. Upon normalizing the NaOH concentrations, it is observed that the Pt and MnMo/Ti cases demonstrate comparable values. However, it is noteworthy that the DE-MnMo/Ti configuration yields the highest NaOH production (**Figure 11 (b)**).

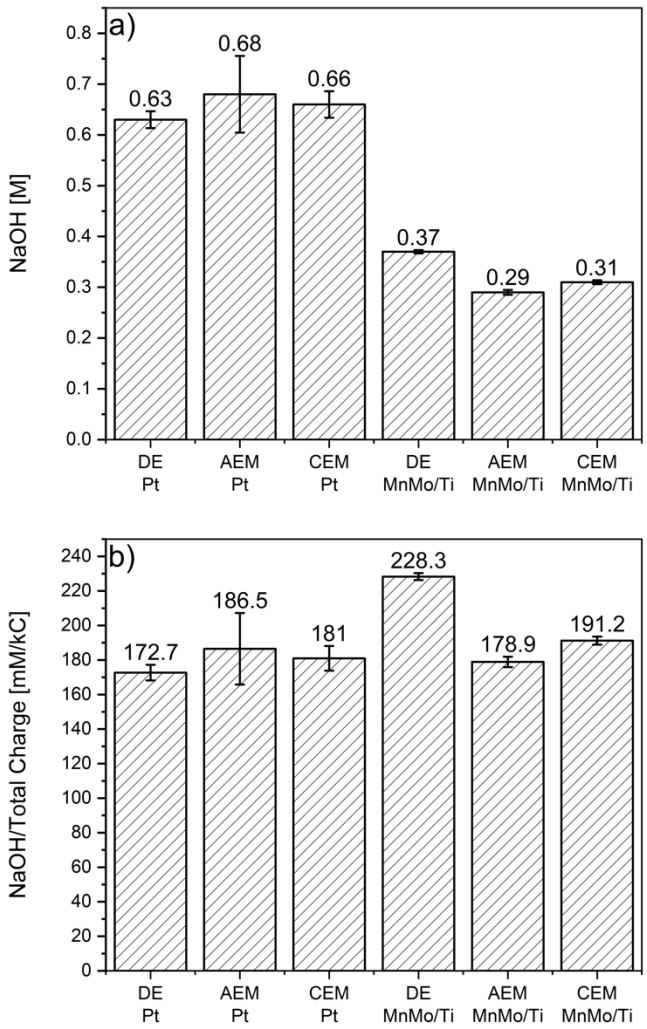

Figure 11. Comparison of NaOH concentration at Pt and MnMo/Ti anodes in different electrolysis systems (a) Concentration of NaOH produced at the Pt and MnMo/Ti anodes in Direct Electrolysis (DE), Anion Exchange Membrane Electrolysis (AEM) and Cation Exchange Membrane Electrolysis (CEM) systems (b) Normalized concentration of NaOH produced at the Pt and MnMo/Ti anodes in Direct Electrolysis (DE), Anion Exchange Membrane Electrolysis (AEM) and Cation Exchange Membrane Electrolysis (CEM) systems.

However, the overall concentrations of HCl are all lower than those of NaOH. As displayed in **Figure 12 (a)**, the concentrations of produced HCl are in the range of 0.04M to 0.25M, which is significantly lower than the range of 0.31M to 0.63M

(NaOH). These results are due to the back diffusion phenomenon, wherein the proton produced in the anode chamber moves to the middle chamber. This phenomenon occurs when there is a gradient of proton concentration across the anion exchange membrane, causing some protons to be transported back across the membrane to the side with lower proton concentration.[27]

Also, to ensure data comparability, normalization of the HCl concentrations is crucial. The graph illustrating the normalized HCl concentrations reveals that the DE-MnMo/Ti configuration yields the highest concentration of HCl among the tested cases (**Figure 12 (b)**). However, the CEM system produced the lowest amount of HCl, regardless of the type of anode used. This phenomenon can be explained by the fact that the CEM anolyte is composed of NaCl at a concentration of 0.86M, which results in a higher initial concentration of Cl^- when compared to the DE and AEM systems (with a Cl^- concentration of 0.05M). As a result, a significant amount of chlorine gas is generated, which in turn reduces the amount of HCl produced.

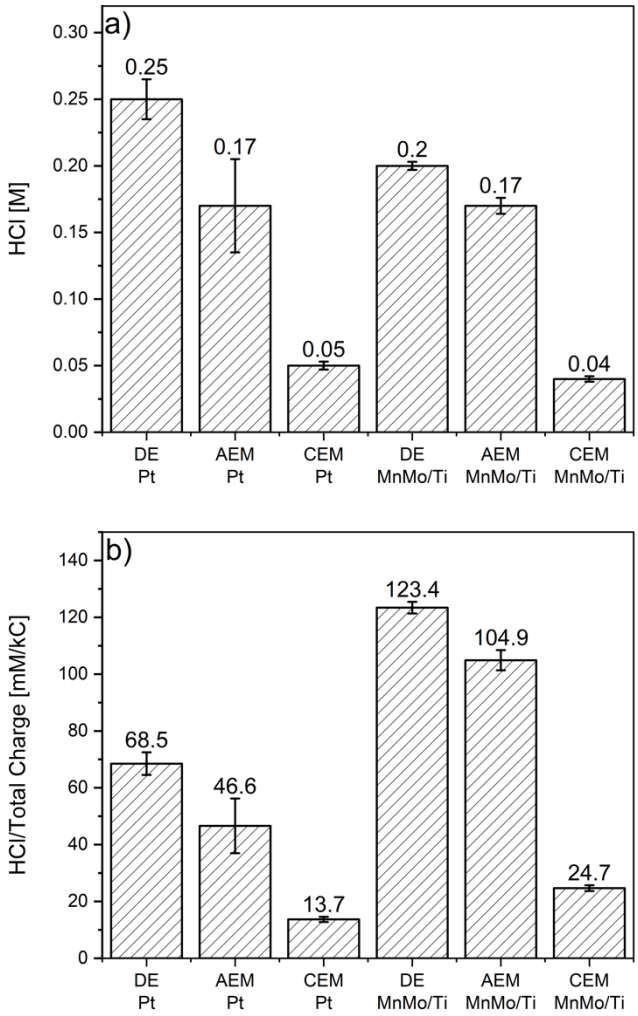

Figure 12. Comparison of HCl concentration at Pt and MnMo/Ti anodes in different electrolysis systems (a) Concentration of HCl produced at the Pt and MnMo/Ti anodes in Direct Electrolysis (DE), Anion Exchange Membrane Electrolysis (AEM) and Cation Exchange Membrane Electrolysis (CEM) systems (b) Normalized concentration of HCl produced at the Pt and MnMo/Ti anodes in Direct Electrolysis (DE), Anion Exchange Membrane Electrolysis (AEM) and Cation Exchange Membrane Electrolysis (CEM) systems.

3.3 H_2 Production under Different Scenarios

All brine electrolysis experiments were conducted with a current density of 90mA/cm^2 for 5 hours. For the Pt cases, the anode surface area was 2.25 cm^2, and total charge of 3,647 C was supplied for each test. In the MnMo/Ti case, the anode area was 1 cm^2, and 1,621 C was supplied. Hydrogen production is influenced by the number of electrons passing through the cathode. Therefore, the theoretically calculated hydrogen production is 0.51 L for the Pt cases and 0.22 L for the MnMo/Ti cases (**Figure 13 (a)**). To establish a baseline, an electrolysis experiment with pure water electrolysis experiment was carried out without membranes with 0.2 M H_2SO_4 and a volume of 150 ml. At the end of the electrolysis, 0.4 L of H_2 was obtained in the end of electrolysis, which is close to the theoretical maximum.

Additionally, normalizing the hydrogen volume is essential for accurate comparison. Upon normalization, it becomes evident that the theoretical hydrogen volume for both the Pt and MnMo electrodes is similar, as depicted in **Figure 13 (b)**. The calculated efficiencies of hydrogen production at the Pt anode range from 79% to 81% with the normalized value. The highest levels of H_2 evolution were obtained from the DE system at the Pt anode (81%), followed by the CEM, and with the AEM system producing the smallest quantity of hydrogen. In contrast, the hydrogen production efficiencies of MnMo/Ti anode were found to be in the range of 35% to 54% with the normalized value, which was much lower than those of Pt anode. Compared to systems using CEM and AEM, DE systems exhibited the best performance (54%) using MnMo/Ti anode. The low efficiency of H_2 production at MnMo/Ti can be caused by the degradation of electrodes during operation. The degraded electrodes can

significantly damage their reactivity to the desired reaction and lead to a decrease in Faradaic efficiency. In some scenarios involving electrode degradation, it was found that the MnMo/Ti coating on the surface of the titanium electrode had detached and settled to the bottom of the cell.

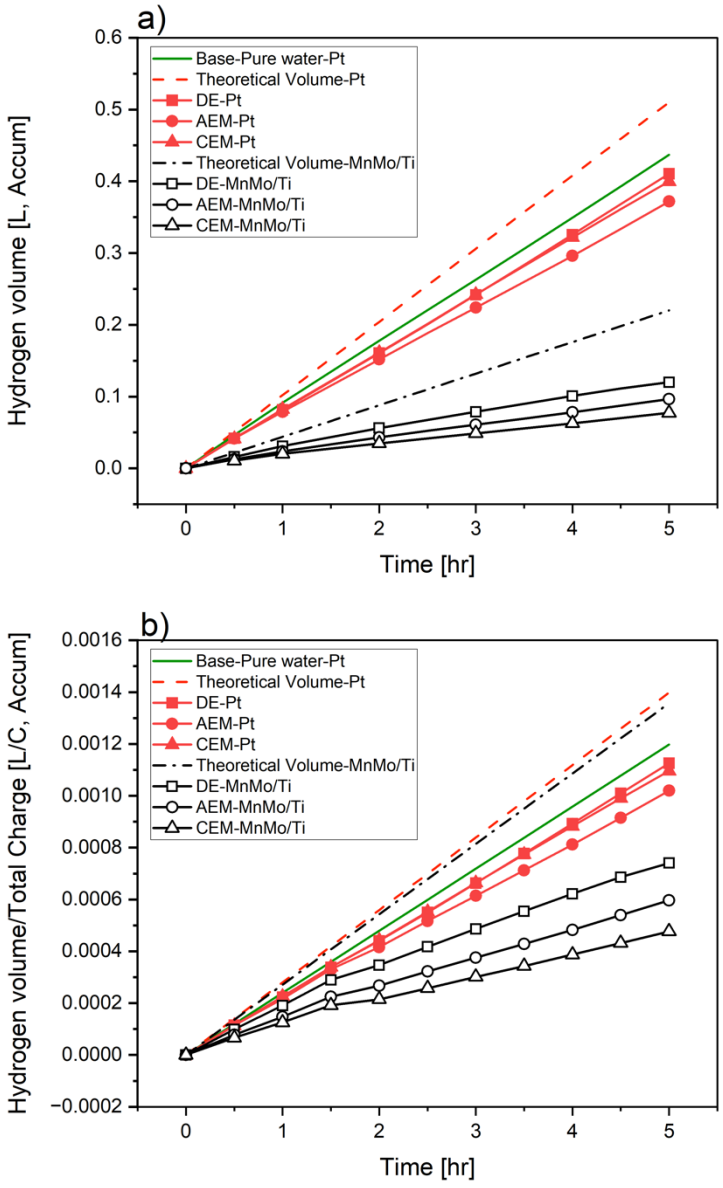

Figure 13. Comparison of hydrogen volume at Pt and MnMo/Ti anodes in different electrolysis systems (a) Hydrogen volume produced at the Pt and MnMo/Ti anodes for Direct Electrolysis (DE), Anion Exchange Membrane Electrolysis (AEM) and Cation Exchange Membrane Electrolysis (CEM) system (b) Normalized hydrogen volume produced at the Pt and MnMo/Ti anodes for Direct Electrolysis (DE), Anion Exchange Membrane Electrolysis (AEM) and Cation Exchange Membrane Electrolysis (CEM) systems.

3.4 Oxygen Evolution Efficiency under Different Scenarios

In the experiments involving the production of chlorine gas and oxygen gas at the anode side via electrolysis, it is assumed that all the generated electrons are utilized in the production of these gases. The oxygen evolution efficiency was examined to evaluate the effectiveness of Cl_2 suppression, as it competes with the CER. As displayed in **Figure 14**, the highest oxygen evolution efficiency of 98.1% was observed in the CEM-MnMo/Ti system, while both the DE and AEM systems showed similar results at around 96%. However, the oxygen evolution efficiency was lower in the Pt case compared to MnMo/Ti, with the highest oxygen evolution efficiency observed in the order of AEM, DE, and CEM. These results show that CEM-Pt produced the highest proportion of Cl_2. Thus, all these results indicate that MnMo/Ti anode can effectively suppress CER.

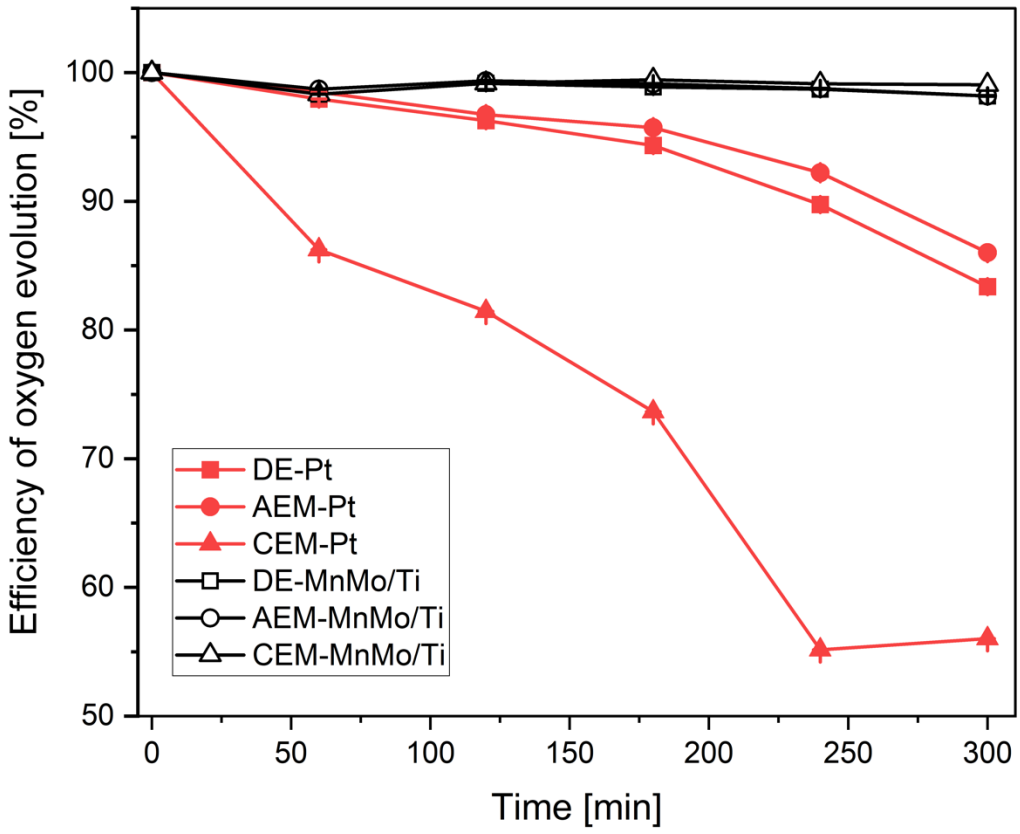

Figure 14. Efficiencies of oxygen evolution at the Pt and MnMo/Ti anodes for Direct Electrolysis (DE), Anion Exchange Membrane Electrolysis (AEM) and Cation Exchange Membrane Electrolysis (CEM) systems.

3.5 Energy Consumption under Various Catalysts and Membrane Scenarios

Energy consumption for brine electrolysis scenarios were determined for various scenarios. **Table 9** shows that the DE system has the lowest energy consumption of 2.8 Wh when using a Pt electrode. Nevertheless, the AEM and CEM systems have similar energy consumptions of 2.8 Wh and 3.2 Wh, respectively, indicating that having fewer membranes does not necessarily result in lower energy consumption compared to DE. When using MnMo/Ti electrodes, a higher voltage is required to achieve the same current density, resulting in a higher energy consumption. The result

shows that the MnMo/Ti electrode consumes slightly more energy than the Pt electrode, due to its smaller electrode surface area of 1 cm^2 compared to 2.25 cm^2 for Pt. To facilitate a comprehensive comparison among the different experimental conditions, the energy consumption values were normalized with respect to the produced NaOH. This normalization approach ensures a fair assessment of energy efficiency. The results indicate that the utilization of MnMo/Ti electrodes led to higher energy consumption compared to Pt electrodes. Notably, the DE system demonstrated the lowest energy consumption among the MnMo/Ti scenarios.

Table 9. Energy consumption for brine electrolysis using Pt and MnMo/Ti electrodes in various configurations including Direct Electrolysis (DE), Cation Exchange Membrane (CEM), and Anion Exchange Membrane (AEM).

Anode	System	Average Potential [v]	Current Density [mA/cm^2]	HCl Concentration		NaOH Concentration		System Energy Consumption [Wh]	Normalized Energy Consumption [kWh/kg_{NaOH}]
				Initial [M]	Final [M]	Initial [M]	Final [M]		
Pt	Base	2.6	90	-	-	-	-	2.6	n.a
Pt	DE	2.7	90	0.05	0.3	0.05	0.68	2.8	2.2
Pt	AEM	2.8	90	0.05	0.22	-	0.68	2.8	2.1
Pt	CEM	3.2	90	-	0.05	0.05	0.71	3.2	2.4
MnMo /Ti	DE	5.9	90	0.05	0.25	0.05	0.42	2.7	3.6
MnMo /Ti	AEM	7.0	90	0.05	0.22	-	0.29	3.1	5.3
MnMo /Ti	CEM	5.8	90	-	0.04	0.05	0.36	2.6	4.2

The DE system has a great potential to improve energy efficiency and, as a result, save energy. As shown in **Figure 15**, when using Pt as the anode, the DE system consumes less energy consumption (2.2 kWh) to produce 1 kg NaOH compared to BMED (3.6kWh). However, when MnMo/Ti is used as the anode in DE system, the same energy consumption as BMED is required due to the overall decrease in reactivity.

These results suggest the need for developing novel anode materials to reduce the energy consumption of the DE system. Anode materials should be elaborately constructed to favor OER reactions over CER reactions to achieve this goal.[24]

Moreover, the energy consumption of AEM and CEM was as high as that of the DE system, even though they used fewer membranes than DE or BMED. This observation explained by the fact that AEM and CEM use NaCl solution as the catholyte and anolyte respectively. The initial pH of a NaCl solution is between 6 and 7.3, but it changes to base in AEM and acid in CEM as the reaction progresses. These changes in pH lead to a higher energy consumption. During brine electrolysis, the HER and OER are the main reactions, and their rates and thermodynamic potentials are pH dependent. The HER reaction is favored at low pH, while the OER reaction is favored at high pH.[8] If the pH of the electrolyte changes significantly during the electrolysis process, the relative rates of the HER and OER reactions can shift, leading to an imbalance in the production of hydrogen and oxygen gases. This change can result in a lower Faradaic efficiency and higher energy consumption.

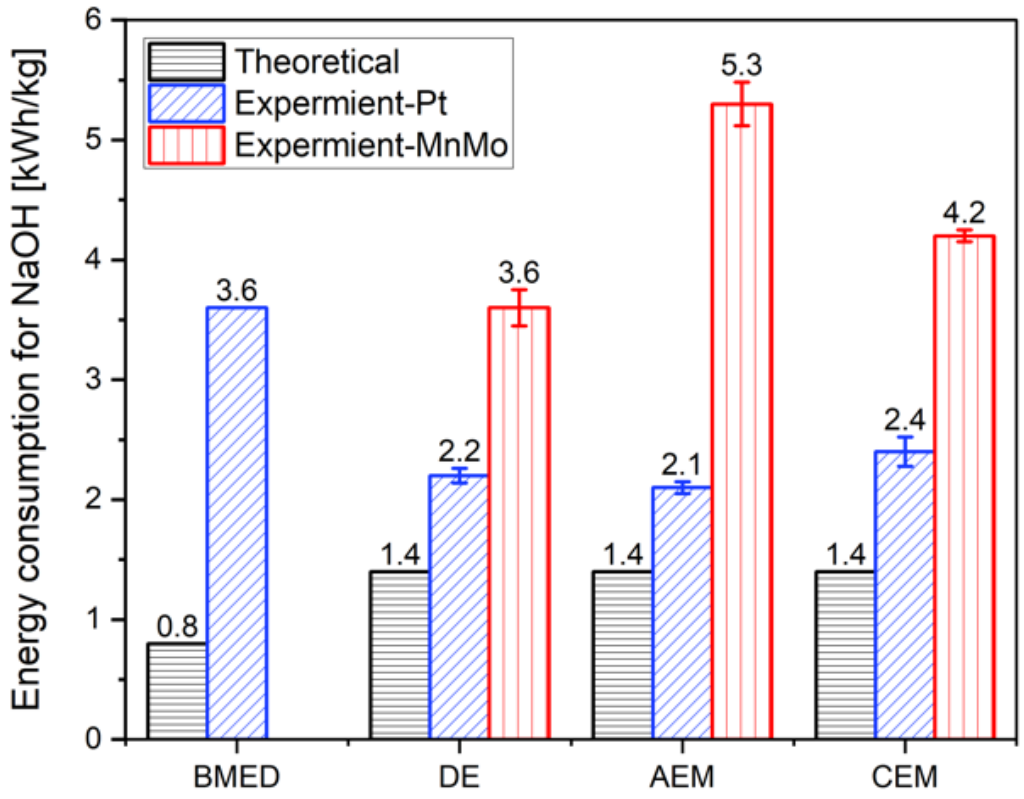

Figure 15. Comparison of theoretical and experimental energy consumption for NaOH production using Bipolar-Membrane Electrodialysis (BMED), Direct Electrolysis (DE), Anion Exchange Membrane Electrolysis (AEM) and Cation Exchange Membrane Electrolysis (CEM) systems. Experimental energy consumption for BMED was determined by Reig et al[20]. Theoretical estimates for DE, AEM and CEM are based on voltages, and they are reported by Kumar et al[24].

CHAPTER 4

ASSESSMENT OF THE ECONOMIC POTENTIAL OF BRINE ELECTROLYSIS FOR CO-PRODUCING H_2, O_2, HCl AND NaOH

In this study, the economic potential of co-producing H_2, O_2, HCl and NaOH via direct electrolysis is contrasted with CEM and AEM as discussed in detail in the following sections.

4.1 Cost of Producing Hydrogen

Hydrogen production costs vary based on the types of electrolysis (e.g., DE, AEM, and CEM) and electrodes used. **Figure 16** illustrates the cost of producing hydrogen per kilogram. Conventional hydrogen production method is steam methane reforming (SMR) using natural gas. The cost is USD 1.3/kg. In case of water electrolysis, alkaline electrolysis has the lowest cost at USD 2/kg, followed by proton exchange membrane electrolyzer (PEM) at USD 2.8/kg. The cost of anion exchange membrane electrolyzer (AEM) and solid oxide electrolyzer cell (SOEC) is higher at USD 19.8/kg and USD 7.7/kg respectively, as these technologies are not as mature and have a shorter lifetime (AEM has a lifetime of 0.6 years and SOEC has a lifetime of 2.3 years). In the case of brine electrolysis, the cost per kilogram of hydrogen varies based on the type of electrode used. With the use of a Pt electrode, the costs are USD 5.7/kg, USD 6.4/kg, USD 6.8/kg for DE, AEM, and CEM respectively. Although the cost is higher compared to freshwater electrolysis, it is worth noting that the brine electrolysis system also produces valuable by-products such as NaOH and HCl These by-products can help offset the costs associated with hydrogen production. When using MnMo/Ti

electrodes, the cost increases significantly to USD 8.3/kg, USD 12.1/kg, and USD 12.7/kg for DE, AEM, and CEM respectively. This is due to the degradation of MnMo/Ti electrodes, which results in the higher energy consumption required to produce the desired products.

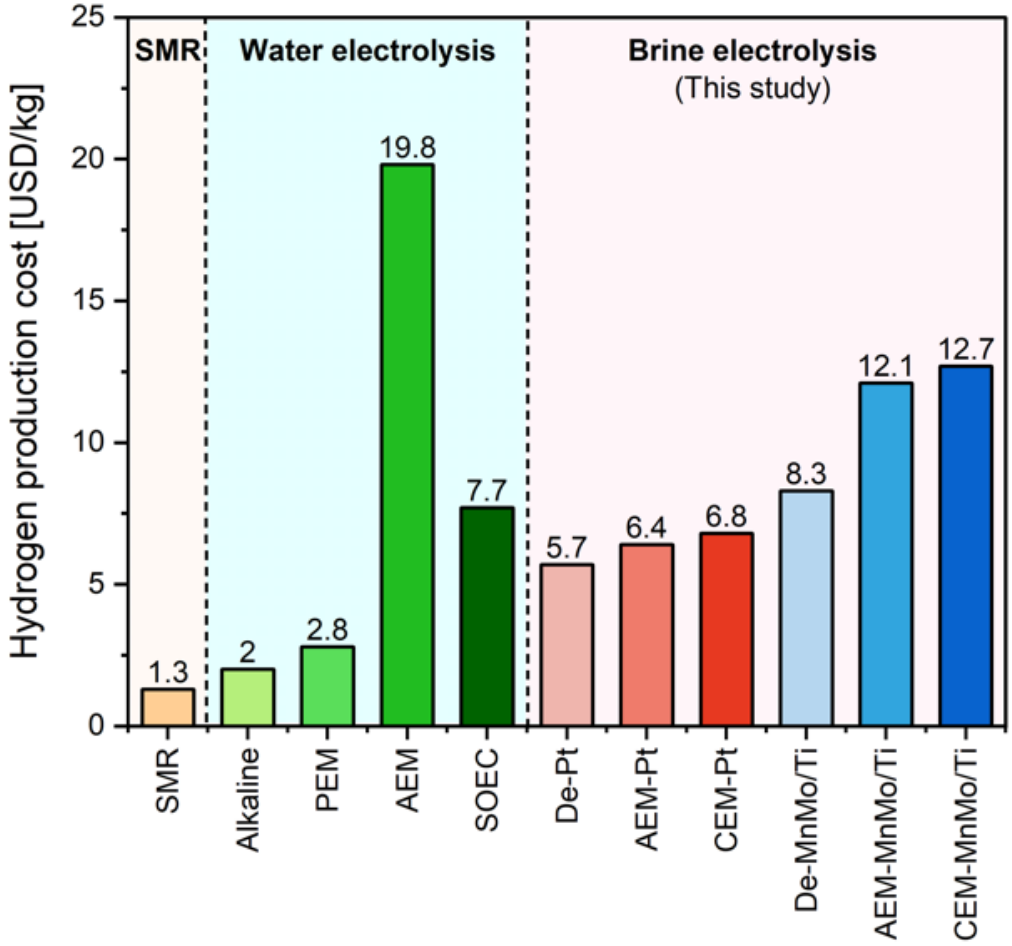

Figure 16. Comparison of H_2 production costs assuming 1MW electrolyzer. Capital costs for Steam Methane Reforming (SMR), Alkaline Electrolysis (Alk), Proton Exchange Membrane Electrolysis (PEM), Anion Exchange Membrane Electrolysis (AEM), Solid Oxide Electrolyzer Cell (SOEC) are reported in published literature.[27] Costs for Direct Electrolysis (DE), Anion Exchange Membrane Electrolysis (AEM) and Cation Exchange Membrane Electrolysis (CEM) using Pt and MnMo/Ti anodes are estimated based on results conducted in this study. Assumptions underlying these calculations are noted in Table 10-11.

Hydrogen production cost can be calculated by Equation (24) and assumptions in **Table 10.**

$$\frac{\text{Cost for electrolyzer [USD]}}{\text{Estimated } H_2 \text{ production during lifetime [kg]}} = \frac{\text{Capital cost } [\frac{\text{USD}}{\text{kW}}] \times 1000\text{kW}}{\text{Produced electricity [kWh]/Electricity efficiency } [\frac{\text{kWh}}{\text{kg } H_2}]} = \frac{\text{Capital cost } [\frac{\text{USD}}{\text{kW}}] \times 1000\text{kW}}{(1000\text{kW} \times 8760\frac{\text{hr}}{\text{yr}} \times \text{Capacity factor} \times \text{Lifetimeyr [yr]})/\text{Electricity efficiency } [\frac{\text{kWh}}{\text{kg } H_2}]} \quad (24)$$

Table 10. Assumptions for economic evaluation of various electrolysis pathways

Electrolyzer capacity [Mw]		1	
Capital cost [USD/kW]	Alkaline, PEM, AEM, SOEC	1,000[28],1,400[28], 931[29], 2000[28]	Water electrolysis
	DE, AEM, CEM	1,400, 1,400, 1,400	Brine electrolysis
Lifetime [yr]	Alkaline, PEM, AEM, SOEC	6.9[28], 7.4[28], 0.6[28], 2.3[28]	Water electrolysis
	DE, AEM, CEM	7, 7, 7	Brine electrolysis
Capacity factor [%]		65[30]	-
H_2 sales price [USD/kg]		6.7	On Dec 22 in US
O_2 sales price [USD/kg]		0.04[31]	
NaOH sales price [USD/kg]		0.46	2017 in US
HCl sales price [USD/kg]		0.11	2017 in US

Table 11. Electrical efficiency for H_2 production

Types of electrolysis		Electrical efficiency [kWh/kg H_2]	H_2 production cost [USD/kg]
Steam methane reforming		-	1.3[31]
Water electrolysis	Alkaline	78 [28]	2.0
	PEM	93 [28]	2.8
	AEM	69 [28]	19.8
	SOEC	50 [28]	7.7
Brine electrolysis	DE-Pt	162 (experiment data)	5.7
	AEM-Pt	183 (experiment data)	6.4
	CEM-Pt	194 (experiment data)	6.8
	DE-MnMo/Ti	235 (experiment data)	8.3
	AEM-MnMo/Ti	344 (experiment data)	12.1
	CEM-MnMo/Ti	362 (experiment data)	12.7

4.2 Estimated Cost and Revenue for Various Routes to Produce H_2

The techno-economic feasibility of brine electrolysis can be improved by the co-production of base and acid. As shown in **Figure 17**, the economic feasibility can be significantly improved through the sale of by-products such as O_2, NaOH and HCl. This improvement is primarily caused by the coproduction of NaOH, which accounts for the majority of the additional revenue generated. In fact, even in the MnMo/Ti case, which has high energy consumption, it exhibits much better economic feasibility than Alkaline and PEM when using freshwater. Using DE-MnMo/Ti electrode and brine, the revenue generated per year is 4 times higher than that of alkaline electrolysis using pure water. This change can be attributed to the co-production of value-added products such as NaOH and HCl.

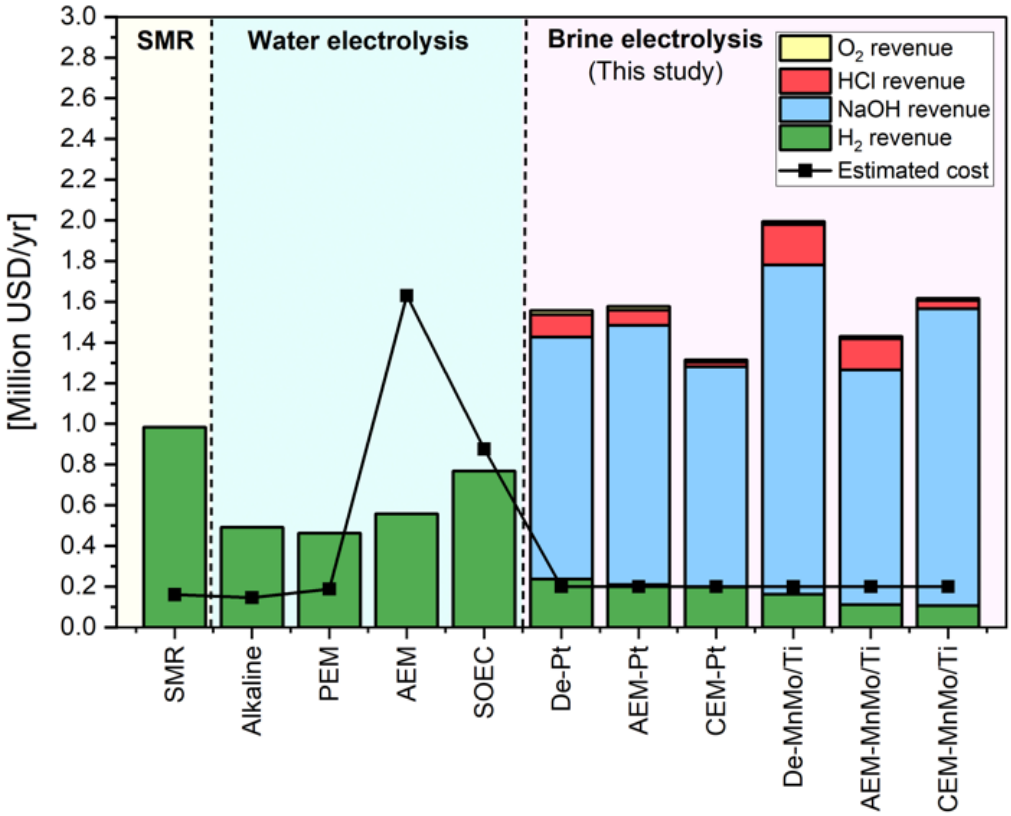

Figure 17. Estimated revenue and costs for using electrolysis routes assuming that 1MW electrolyzer is used. Assumptions underlying this calculation are noted in Table 12-15.

The cost estimate for one year can be determined using Equation (25), based on the assumptions from **Table 13**. The results are presented in **Table 12**.

$$\begin{aligned}\frac{\text{Estimated cost}}{\text{yr}} &= \text{H}_2\ \text{productioncost}\left[\frac{\text{USD}}{\text{kg}}\right] \times \text{H}_2\ \text{production}\left[\frac{\text{kg}}{\text{yr}}\right] \\ &= \text{H}_2\ \text{productioncost}\left[\frac{\text{USD}}{\text{kg}}\right] \times \left(\frac{\text{Produced electricity [kWh]}}{\text{yr}} / \text{Electricity efficiency}\left[\frac{\text{kWh}}{\text{kg H}_2}\right]\right) \\ &= \text{H}_2\ \text{production cost}\left[\frac{\text{USD}}{\text{kg}}\right] \times \left(\frac{1000\text{kW} \times 8760\frac{\text{hr}}{\text{yr}} \times \text{Capacity factor}}{\text{yr}} / \text{Electricity efficiency}\left[\frac{\text{kWh}}{\text{kg H}_2}\right]\right)\end{aligned} \quad (25)$$

Table 12. Estimated costs for producing H_2 via water and brine electrolysis when a 1 MW electrolyzer is operated for a year.

Types of electrolysis		H_2 production cost [USD/kg]	H_2 production [kg/yr]	Total cost [USD/yr]
Steam methane reforming		1.3 [32]	146,000	16,600
Water electrolysis	Alkaline	2.0	73,000	146,000
	PEM	2.8	68,602	188,677
	AEM	19.8	82,522	1,631,112
	SOEC	7.7	113,880	876,000
Brine electrolysis	DE-Pt	5.7 (experiment data)	35,148	200,000
	AEM-Pt	6.4 (experiment data)	31,115	200,000
	CEM-Pt	6.8 (experiment data)	29,351	200,000
	DE-MnMo/Ti	8.3 (experiment data)	24,207	200,000
	AEM-MnMo/Ti	12.1 (experiment data)	16,575	200,000
	CEM-MnMo/Ti	12.7 (experiment data)	15,730	200,000

The estimated revenue for one year can be calculated using Equation (26) and assumptions in **Table 12**, which requires the yields of H_2, O_2, NaOH, and HCl produced when operating a 1MW electrolyzer. The production of H_2 can be calculated using hydrogen electrical efficiency in **Table 13**. Based on the ratios in **Table 14**, it is possible to predict the yields of H_2, O_2, NaOH, and HCl produced by a 1MW electrolyzer (**Table 15**).

$$\frac{\text{Estimated revenue}}{\text{yr}} = \frac{\text{H}_2 \text{ revenue} + \text{NaOH revenue} + \text{HCl revenue}}{\text{yr}} \quad (26)$$

Table 13. Electrical efficiencies and associated costs for H_2 production via water and brine electrolysis

Types of electrolysis		Electrical efficiency [kWh/kg H_2]	H_2 production cost [USD/kg]
Steam methane reforming		-	1.3[31]
Water electrolysis	Alkaline	78 [28]	2.0
	PEM	93 [28]	2.8
	AEM	69 [28]	19.8
	SOEC	50 [28]	7.7
Brine electrolysis	DE-Pt	162 (experiment data)	5.7
	AEM-Pt	183 (experiment data)	6.4

	CEM-Pt	194 (experiment data)	6.8
	DE-MnMo	235 (experiment data)	8.3
	AEM-MnMo	344 (experiment data)	12.1
	CEM-MnMo	362 (experiment data)	12.7

Table 14. Estimated yields of H_2 and byproducts. Results are based on experimental data.

Brine electrolysis	Experiment Data				Expected weight			
	H_2 [mol]	O_2 [mol]	NaOH [mol]	HCl [mol]	H_2 [kg]	O_2 [kg]	NaOH [kg]	HCl [kg]
DE-Pt	0.017	0.0079	0.031	0.013	1	15	73	28
AEM-Pt	0.0154	0.0081	0.034	0.009	1	15	88	21
CEM-Pt	0.0166	0.0053	0.033	0.003	1	10	79	7
DE -MnMo/Ti	0.011	0.009	0.041	0.023	1	17	144	73
AEM -MnMo/Ti	0.009	0.009	0.034	0.020	1	17	150	82
CEM -MnMo/Ti	0.007	0.009	0.036	0.005	1	18	200	23

Table 15. Estimated yields and revenue of H_2 and byproducts (e.g., O_2, NaOH, and HCl) using a 1MW electrolyzer is operated for a year.

Types of electrolysis		Production				Expected revenue			
		H_2 [kg/yr]	O_2 [kg/yr]	NaOH [kg/yr]	HCl [kg/yr]	H_2 [USD/yr]	O_2 [USD/yr]	NaOH [USD/yr]	HCl [USD/yr]
Steam methane reforming		146,000	-	-	-	984,916	-	-	-
Water electrolysis	Alkaline	73,000	-	-	-	492,458	-	-	-
	PEM	68,602	-	-	-	462,792	-	-	-
	AEM	82,522	-	-	-	556,692	-	-	-
	SOEC	113,880	-	-	-	768,234	-	-	-
Brine electrolysis	DE-Pt	35,148	522,250	2,561,555	979,154	237,109	20,890	1,189,842	109,910
	AEM-Pt	31,115	474,024	2,745,447	662,433	209,900	18,961	1,275,260	74,358
	CEM-Pt	29,351	292,577	2,331,901	193,234	197,999	11,703	1,083,168	21,690
	DE -MnMo/Ti	124,207	420,006	3,482,827	1,763,700	163,300	16,800	1,617,773	197,975
	AEM -MnMo/Ti	16,575	287,582	2,484,087	1,358,575	111,813	11,503	1,153,859	152,500
	CEM -MnMo/Ti	15,730	279,576	3,143,249	358,141	106,112	11,183	1,460,039	40,201

These analyses demonstrate that DE with Pt and MnMo/Ti electrodes can be economically competitive with other approaches to produce H_2 when the value occurred from co-product generation is considered.

CHAPTER 5

ASSESSMENT OF THE LIFE CYCLE IMPACTS OF BRINE ELECTROLYSIS FOR CO-PRODUCING H2, O2, HCl, and NaOH

The life cycle impacts of co-producing H_2, O_2, HCl, and NaOH via brine electrolysis using the experimental analyses presented in the previous chapters are discussed in this section.

5.1 Life Cycle Assessment of Brine-DE-MnMo/Ti Process

This study aims to determine the environmental impact of the process of generating higher concentrations of hydrochloric acid, sodium hydroxide, oxygen and hydrogen from brine. To achieve this objective, the Life Cycle Assessment (LCA) framework will be used to evaluate the environmental impacts in three life cycle impact categories: energy usage, carbon footprint, and water usage. Through this evaluation, a deeper understanding of the impacts will be gained, providing valuable insights for decision-making and identifying opportunities for future improvements.

5.1.1 Scope

The scope of this LCA will be limited to the process of generating higher concentrations of hydrochloric acid, sodium hydroxide, oxygen and hydrogen from brine. This means that the raw material extraction and end-of-life components of the system will not be the primary components of emphasis in this study. Specifically, the LCA analysis will focus solely on the DE MnMo/Ti system, as depicted in **Figure 18**. The system boundaries for this analysis will be defined as the exterior of the processes, including the membrane, anode-cathode, and electrochemical cell tank, as shown in **Figure 18**. Moreover, the LCA results compare the environmental impact of the DE-

MnMo/Ti systems with the production of 1 metric ton of hydrochloric acid using traditional methods. This comparison enables a comprehensive assessment of the environmental implications associated with the investigated system of interest in relation to the conventional approaches.

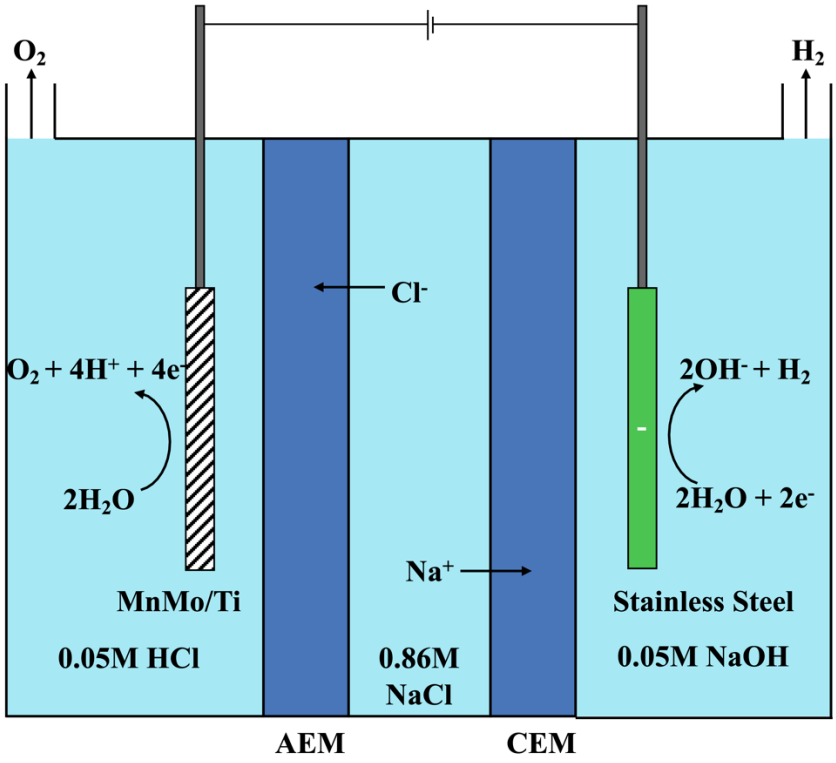

Figure 18. Schematic representation of the Direct Electrolysis (DE) process with MnMO/Ti electrode.

5.1.2 Life Cycle Inventory

The Life Cycle Inventory Assessment (LCI) for this study comprises two key processes. The first process involves the formation of the MnMo/Ti electrode, which produces the MnMo/Ti electrode used in the brine electrolysis process. This process requires heat, electricity, a titanium anode, and solutions of manganese sulfate and sodium molybdate. Additionally, platinum is used in the production of the MnMo/Ti electrode, which can be reused several times. The second process is the brine electrolysis process,

which produces hydrochloric acid, sodium hydroxide, and hydrogen gas, along with chlorine gas. This process requires low concentrations of hydrochloric acid and sodium hydroxide, as well as a sodium chloride solution and a stainless steel cathode, with electricity being used to drive the reaction.

In this study, two scenarios were evaluated to determine the environmental impacts of the process: one using market-based energy and the other using solar energy. The Life Cycle Assessment (LCA) model was created in SimaPro 9.4.0.2 using the IMPACT World+ Midpoint 1.2 method. Three impact categories were considered in the analysis: climate change, measured using Global Warming Potentials on a 100-year time frame (GWP100) in kg CO_2-equivalents; fossil and nuclear energy use, measured in MJ deprived; and water scarcity impact, measured in m^3 world equivalent.

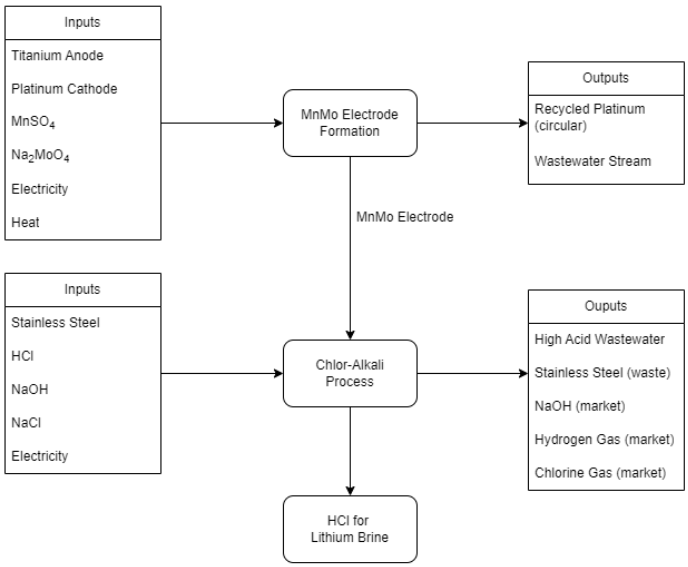

Figure 19. Process flow diagram and phase boundary for brine electrolysis system. The mass balance calculations for this life cycle inventory are based on the production of 1 kg of hydrochloric acid and are determined using experimental data. These numbers were then scaled up to 1,000 kg for the Life Cycle Impact Assessment.

5.1.3 Assumptions and Limitations

In this LCA analysis, certain assumptions and limitations have been made. Firstly, the recycling of the used MnMo/Ti electrode was not considered, and a new titanium anode is assumed to be used for each MnMo/Ti electrode formation process. Second, while the platinum cathode can be recycled several times in this process, it has not been included in this LCA analysis as it will need to be considered in a full cradle-to-gate, full life cycle analysis. Additionally, the assumption is made that the stainless steel used in the process is recycled and sold to the market as scrap. The production of manganese sulfate and sodium molybdate solutions is assumed for each process, and a recycling stream has not been considered. Furthermore, the handling of wastewater from this process has not been included in the analysis. The assumption is made that sodium hydroxide, hydrogen, oxygen and chlorine are all stored and sold to the market. It is also important to note that this LCA analysis is conducted on a process that has been validated at the laboratory scale and does not include sensitivity or risk analysis for large-scale process deployment. The environmental impacts for the creation and end-of-life of the functional blocks, such as the AEM membrane and CEM membrane, will not be utilized in this LCA model.

5.2 Environment Impacts

Life Cycle Assessment (LCA) was used to evaluate the environmental impacts in three life cycle impact categories: energy usage, carbon footprint, and water usage. The results, depicted in **Figure 20**, provide a comparison of the environmental impact between the DE-Brine system and traditional methods of producing 1 metric ton of HCl. Two scenarios were considered: utilizing electricity from the market and

utilizing solar energy. Even when buying electricity from the market, the environmental impact is positive. The lab-scale experiments require several materials, such as stainless steel, MnMo/Ti electrode, low concentrations of HCl, NaOH, brine, and electricity, all of which have positive effects in terms of carbon footprint, energy use, and water usage. However, after brine electrolysis, H_2, O_2, NaOH, HCl, and a small amount of chlorine gas are produced, and stainless steel is sold as scraps and recycled. Overall, a net positive environmental impact is noted from these studies. The DE-Brine system, employing MnMo/Ti electrodes using solar energy, demonstrates significant environmental benefits. The results indicate a reduction in greenhouse gas emissions by 920 kg CO_2 eq, a decrease in energy use by 19,279 MJ, and a decrease in water usage by 17,175 m^3. These findings suggest that the DE-Brine system has the potential to achieve carbon neutrality or even carbon negativity when powered by market energy or solar energy.

Regarding energy usage, the presence of sodium hydroxide as a byproduct indicates that the DE MnMo/Ti system is environmentally friendly in terms of energy use. The utilization of this system can help mitigate the need for additional sodium hydroxide production since a substantial amount is already generated as a byproduct. Furthermore, with regard to water usage, it is crucial to implement effective steel recycling practices to ensure a net negative impact. Further research on recycling stainless steel from experiments and handling of wastewater should be considered to enhance the sustainability of the overall system. Additionally, future Life Cycle Assessments should employ more rigorous assumptions and methodologies to provide

a comprehensive evaluation of the system's environmental impact. In conclusion, the DE-Brine system utilizing MnMo/Ti electrodes serves as a promising example of how the adoption of sustainable practices can yield both economic and environmental benefits.

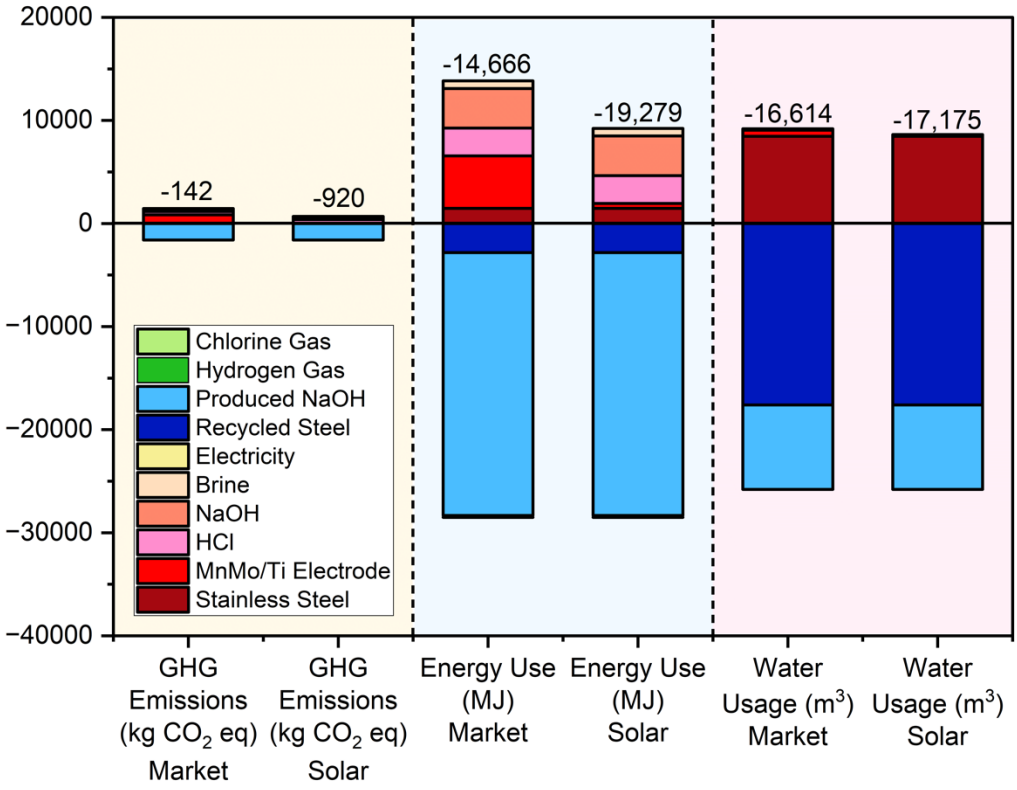

Figure 20. Life cycle impacts on greenhouse gas emissions (GHG), energy use and water usage using MnMo/Ti anode and stainless steel cathode for direct electrosynthesis (DE) of brine, with a production scale of 1 metric ton of hydrochloric acid.

CHAPTER 6

CONCLUSION

The results of this study provide valuable insights into the co-recovery of multiple value-added products (e.g., H_2, O_2, NaOH, and HCl) via brine electrolysis using various configurations including Direct Electrolysis (DE) without bipolar membranes, Cation Exchange Membranes (CEM), and Anion Exchange Membranes (AEM) using Pt and MnMo/Ti electrodes. The challenge of suppressing Cl_2 evolution with Pt electrodes was effectively addressed through the development of the MnMo/Ti electrode, which demonstrated superior performance in suppressing Cl_2 production at the anode, making it a promising alternative to Pt electrodes. The experimental findings revealed that the DE-MnMo/Ti configuration exhibited the highest production of NaOH and HCl when the results were normalized. However, it was observed that the MnMo electrode experienced degradation, which could contribute to higher energy consumption. In case of hydrogen production, Pt cases showed better performance compared to MnMo/Ti cases. When considering the economic potential of MnMo/Ti electrodes, the cost of hydrogen production is higher due to higher energy penalty, but the economic feasibility can be improved through the production of NaOH and HCl. Furthermore, the LCA results show that the DE-brine system using MnMo/Ti electrodes has a positive impact on the environment by reducing greenhouse gas emissions by 920 kg CO_2 eq, energy use by 19,279 MJ, and water usage by 17,175 m^3. In conclusion, the findings of this study demonstrate the potential of brine electrolysis as a sustainable and cost-effective approach for hydrogen production in addition to the co-recovery of multiple products (e.g., O_2, NaOH, and HCl). This study provides an

integrated approach to connect experimental studies with detailed TEA and LCA to assess economic and environmental impacts.

CHAPTER 7

Future Work

The future work of this research encompasses several important aspects. The primary focus is to address the issue of degradation observed in the MnMo/Ti electrode during brine electrolysis. While the MnMo/Ti electrode has demonstrated higher production of NaOH and HCl compared to other configurations, its degradation raises concerns about long-term stability and performance. Therefore, it is imperative to investigate and identify alternative materials that can serve as stable catalysts for suppressing chlorine evolution while minimizing degradation. The type of anode material that can be replaced depends on the pH. Researchers have successfully developed anodes composed of $Ti/IrO_2/MnO_2$ that were doped with Mo, W, and Sn in acidic environments.[33] Additionally, a strategy employed to enhance electrode strength and prevent degradation involves applying an intermediate layer of iridium dioxide (IrO_2) onto the titanium substrate. In other studies for this purpose, IrOX nanoparticles have been deposited onto a glassy carbon substrate using electroflocculation, followed by the electrodeposition of MnOx.[33] For medium pH conditions (pH 7-8), Ti/IrO_2/MnOx and Cobalt-phosphate (CoPi) have been employed as alternative anode materials.[33] In high pH conditions (pH 12-14), extensive research is being conducted, with many studies focusing on the use of nickel-based anodes.[33] Furthermore, a detailed investigation into the mechanism of chlorine evolution suppression is necessary. Analyzing the remaining ions in the anolyte through techniques like Inductively Coupled Plasma (ICP) analysis or studying the components of particles detached from the electrode surface can provide valuable insights into the effective suppression of

chlorine evolution. In summary, the main future work involves identifying stable anodic materials to suppress Cl_2 evolution and minimize corrosion as a catalysts, exploring alternative approaches to enhance the MnMo electrode's strength and durability, investigating the mechanism of chlorine evolution suppression, and optimizing the DE-Brine system for commercial viability. By addressing these aspects, significant progress can be made in the field of brine electrolysis and hydrogen production.

REFERENCE

1. Allan, R. P., Hawkins, E., Bellouin, N., & Collins, B. (2021). IPCC, 2021: summary for Policymakers.

2. Gowrisankaran, G., Reynolds, S. S., & Samano, M. (2016). Intermittency and the value of renewable energy. *Journal of Political Economy*, *124*(4), 1187-1234.

3. Bielmann, M., Vogt, U. F., Zimmermann, M., & Züttel, A. (2011). Seasonal energy storage system based on hydrogen for self sufficient living. *Journal of Power Sources*, *196*(8), 4054-4060.

4. Davis, S. J., Lewis, N. S., Shaner, M., Aggarwal, S., Arent, D., Azevedo, I. L., ... & Caldeira, K. (2018). Net-zero emissions energy systems. *Science, 360* (6396), eaas9793.

5. Richter, B. D., Abell, D., Bacha, E., Brauman, K., Calos, S., Cohn, A., ... & Siegfried, E. (2013). Tapped out: how can cities secure their water future?. *Water Policy*, *15*(3), 335-363.

6. Janssen, C. H. (2021). Heavy Metal Extractions from NaCl Brines to Pseudoprotic Ionic Liquids. *Industrial & Engineering Chemistry Research*, *60*(4), 1808-1816.

7. Dastgheib, S. A., & Salih, H. H. (2019). Treatment of highly saline brines by supercritical precipitation followed by supercritical membrane separation. *Industrial & Engineering Chemistry Research*, *58*(8), 3370-3376.

8. Kumar, A., Phillips, K. R., Thiel, G. P., Schröder, U., & Lienhard, J. H. (2019). Direct electrosynthesis of sodium hydroxide and hydrochloric acid from brine streams. *Nature Catalysis*, *2*(2), 106-113.

9. Schewe, J., Heinke, J., Gerten, D., Haddeland, I., Arnell, N. W., Clark, D. B., ... & Kabat, P. (2014). Multimodel assessment of water scarcity under climate change. *Proceedings of the National Academy of Sciences*, *111*(9), 3245-3250.

10. Mekonnen, M. M., & Hoekstra, A. Y. (2016). Four billion people facing severe water scarcity. *Science advances*, *2*(2), e1500323.

11. Jones, E., Qadir, M., van Vliet, M. T., Smakhtin, V., & Kang, S. M. (2019). The state of desalination and brine production: A global outlook. *Science of the Total Environment*, *657*, 1343-1356.

12. Arnal, J. M., Sancho, M., Iborra, I., Gozálvez, J. M., Santafé, A., & Lora, J. (2005). Concentration of brines from RO desalination plants by natural evaporation. Desalination, 182(1-3), 435-439.

13. Lin, H. W., Cejudo-Marín, R., Jeremiasse, A. W., Rabaey, K., Yuan, Z., & Pikaar, I. (2016). Direct anodic hydrochloric acid and cathodic caustic production during water electrolysis. *Scientific reports*, *6*(1), 20494.

14. Zhu, W., Fu, X., Wang, A., Ren, M., Wei, Z., Tang, C., ... & Wang, J. (2022). Energy-efficient electrolytic H2 production and high-value added H2-acid-base co-electrosynthesis modes enabled by a Ni2P catalyst in a diaphragm cell. *Applied Catalysis B: Environmental*, *317*, 121726.

15. Herrero-Gonzalez, M., & Ibañez, R. (2022). Technical and Environmental Feasibilities of the Commercial Production of NaOH from Brine by Means of an Integrated EDBM and Evaporation Process. *Membranes*, *12*(9), 885.

16. Liu, Y., Sun, Y., & Peng, Z. (2022). Evaluation of bipolar membrane electrodialysis for desalination of simulated salicylic acid wastewater. *Desalination*, *537*, 115866.

17. Hussain, A., Yan, H., Ul Afsar, N., Jiang, C., Wang, Y., & Xu, T. (2022). Multistage-batch bipolar membrane electrodialysis for base production from high-salinity wastewater. *Frontiers of Chemical Science and Engineering*, *16*(5), 764-773.

18. Herrero-Gonzalez, M., Diaz-Guridi, P., Dominguez-Ramos, A., Irabien, A., & Ibañez, R. (2020). Highly concentrated HCl and NaOH from brines using electrodialysis with bipolar membranes. *Separation and Purification Technology*, *242*, 116785.

19. Chen, Q. B., Wang, J., Liu, Y., Zhao, J., Li, P. F., & Xu, Y. (2021). Sustainable disposal of seawater brine by novel hybrid electrodialysis system: Fine utilization of mixed salts. *Water Research*, *201*, 117335.

20. Reig, M., Casas, S., Valderrama, C., Gibert, O., & Cortina, J. L. (2016). Integration of monopolar and bipolar electrodialysis for valorization of seawater reverse osmosis desalination brines: Production of strong acid and base. *Desalination*, *398*, 87-97.

21. Badjatya, P., Akca, A. H., Fraga Alvarez, D. V., Chang, B., Ma, S., Pang, X., ... & Kawashima, S. (2022). Carbon-negative cement manufacturing from seawater-derived magnesium feedstocks. *Proceedings of the National Academy of Sciences*, *119*(34), e2114680119.

22. Matsui, T., Habazaki, H., Kawashima, A., Asami, K., Kumagai, N., & Hashimoto, K. (2002). Anodically deposited manganese–molybdenum–tungsten oxide anodes for oxygen evolution in seawater electrolysis. *Journal of applied electrochemistry*, *32*, 993-1000.

23. Abdel-Aal, H. K., Sultan, S. M., & Hussein, I. A. (1993). Parametric study for saline water electrolysis: part II—chlorine evolution, selectivity and determination. *International journal of hydrogen energy*, *18*(7), 545-551.

24. Kumar, A., Du, F., & Lienhard, J. H. (2021). Caustic soda production, energy efficiency, and electrolyzers. *ACS Energy Letters*, *6*(10), 3563-3566.

25. Maril, M., Delplancke, J. L., Cisternas, N., Tobosque, P., Maril, Y., & Carrasco, C. (2022). Critical aspects in the development of anodes for use in seawater electrolysis. *International Journal of Hydrogen Energy*, *47*(6), 3532-3549.

26. Vos, J. G., Wezendonk, T. A., Jeremiasse, A. W., & Koper, M. T. (2018). MnOx/IrOx as selective oxygen evolution electrocatalyst in acidic chloride solution. *Journal of the American Chemical Society*, *140*(32), 10270-10281.

27. Vallejo, M. E., Persin, F., Innocent, C., Sistat, P., & Pourcelly, G. (2000). Electrotransport of Cr (VI) through an anion exchange membrane. *Separation and purification technology*, *21*(1-2), 61-69.

28. IRENA, E. (2020). Green hydrogen cost reduction: scaling up electrolysers to meet the 1.5 C climate goal. In */Publications/2020/dec/green-hydrogen-cost-reduction* (p. 105).

29. Ionomr Innovations. (2020). *"WHITE PAPER: Hydrogen Production Cost by AEM Water Electrolysis"*.https://ionomr.com/wpcontent/uploads/2021/02/FM-7024-A-Hydrogen-Production-Cost-by-AEM-White-Paper-copy.pdf

30. Solyanik, A. (2021). Analysis of cost efficiency of hydrogen production via electrolysis: the Russian case study. In E3S Web of Conferences (Vol. 289, p. 04002). EDP Sciences.

31. Dorris, C. C., Lu, E., Park, S., & Toro, F. H. (2016). High-purity oxygen. production using mixed ionic-electronic conducting sorbents.

32. Oni, A. O., Anaya, K., Giwa, T., Di Lullo, G., & Kumar, A. (2022). Comparative assessment of blue hydrogen from steam methane reforming, autothermal reforming, and natural gas decomposition technologies for natural gas-producing regions. *Energy Conversion and Management*, *254*, 115245.

33. Maril, M., Delplancke, J. L., Cisternas, N., Tobosque, P., Maril, Y., &. Carrasco, C. (2022). Critical aspects in the development of anodes for use in seawater electrolysis. International Journal of Hydrogen Energy, 47(6), 3532-3549